Adapting Regenerative Braking Strength to Driver Preference

by

John Francis Marrone

A thesis

presented to the University of Waterloo

in fulfillment of the

thesis requirement for the degree of

Master of Applied Science

in

Mechanical and Mechatronics Engineering

Waterloo, Ontario, Canada, 2023

Author's Declaration

I hereby declare that I am the sole author of this thesis. This is a true copy of the thesis, including any required final revisions, as accepted by my examiners.

I understand that my thesis may be made electronically available to the public.

Abstract

The modern automotive industry has witnessed a growing emphasis on adapting the driving experience to individual drivers. With the rising popularity of electrified vehicles, the implementation of regenerative braking systems, specifically lift-off regenerative braking, has become a focal point. However, research indicates that drivers often find the predefined deceleration response during lift-off regenerative braking to be undesirable. This thesis addresses this issue by developing an adaptive regenerative braking controller that learns driver preferences, thereby fulfilling the objective of enhancing the driving experience of lift-off regenerative braking systems by reducing driver fatigue through the minimization of pedal interventions. The research focuses on three critical aspects: accurate identification of driving conditions, acquisition of driver preferences for lift-off regenerative braking, and compatibility with real-time automotive hardware. By leveraging advanced techniques like HDBSCAN clustering, fuzzy logic inference, and online Q-learning, the research achieves accurate driving condition identification and adaptation to individual driver preferences in a control scheme that can be practically deployed in-vehicle. Real-world testing demonstrates the controller's 80.9 % accuracy in identifying driving conditions as well as its successful learning of the driver's preferred deceleration to within 1.9 %. Subsequently, the adaptive regenerative braking controller results in a 23.2 % reduction in pedal interventions during deceleration compared to a baseline that is representative of an industry-standard implementation of lift-off regenerative braking. This outcome underscores the controller's potential to alleviate driver fatigue and enhance the overall driving experience. This research contributes to the advancement of electrified vehicle powertrain control, focusing on improving driver acceptance and satisfaction with regenerative braking systems.

Acknowledgements

I would like to thank my supervisor Dr. Roydon Fraser for his mentorship throughout my two years as a graduate lead of the University of Waterloo Alternative Fuels Team. His patient guidance throughout countless hours of poring over reports, deliverables, and presentations has been instrumental in cultivating a profound commitment to personal and professional standards within not only myself but also the entire team.

A special thank you to my peers at the University of Waterloo Alternative Fuels Team. Your passion and unyielding dedication to uniting as a team and striving for excellence, even in the face of stressful challenges, has been truly inspiring. I would also like to express my sincere gratitude to the organizers and mentors involved in EcoCAR, especially those from General Motors, Argonne National Laboratory, and MathWorks. Thank you for your boundless support in putting together this exceptional program and investing your time and resources into developing the next generation of automotive engineers.

Dedication

I dedicate this thesis to my parents, John and Milena, whose unwavering support and encouragement have been the cornerstone of my academic journey.

Table of Contents

List of Figures

List of Tables

List of Abbreviations

ADAS	Advanced Driver Assistance Systems
APP	Accelerator Pedal Position
ARB	Adaptive Regenerative Braking
B	Baseline
BPP	Brake Pedal Position
CRB_0.5	Constant Regenerative Braking, 0.5 m/s^2
CRB_1.6	Constant Regenerative Braking, 1.6 m/s^2
DBSCAN	Density-Based Spatial Clustering of Applications with Noise
EPA	Environmental Protection Agency
EV	Electric Vehicle
FHEV	Full Hybrid Electric Vehicle
FIS	Fuzzy Inference System
HBS	Hybrid Braking System
HDBSCAN	Hierarchical Density-Based Spatial Clustering of Applications with Noise
ICE	Internal Combustion Engine
J1015	Japanese 10-15 Drive Cycle
MDP	Markov Decision Process
MHEV	Mild Hybrid Electric Vehicle
MT	Micro-Trip
NYCC	New York City Cycle
UDDS	Urban Dynamometer Driving Schedule
UWAFT	University of Waterloo Alternative Fuels Team
V2X	Vehicle-to-Everything
WLTC	Worldwide Harmonized Light-duty Test Cycle
WCSS	Within-Cluster Sum of Squares

Chapter 1
Introduction

1.1 Research Context

As the automotive industry undergoes a profound transformation towards electrification, the integration of regenerative braking technology plays a pivotal role in redefining how drivers interact with their vehicles as well as the experience of driving as a whole. This section provides an exploration of the research context surrounding electrified vehicles and their utilization of regenerative braking systems before identifying the need for a regenerative braking control system that adapts to the driver's preferences. This section examines the research context related to electrified vehicles and their use of regenerative braking systems. It then highlights the limitations of existing methods of implementing regenerative braking and justifies the need for a regenerative braking control system that can adjust according to the driver's preferences.

1.1.1 Automotive Electrification

The last few decades have witnessed a substantial rise in public consciousness regarding environmental and sustainability challenges. This heightened awareness, coupled with rising gas prices, has translated into a mounting pressure on automotive manufacturers to develop and produce vehicles that prioritize energy efficiency, reduce carbon emissions, and are wholly less dependent on fossil fuels. Many automotive manufacturers are increasingly prioritizing electrification, a process that involves replacing fossil fuel-based technologies with electric ones, as their central strategy to lower emissions across their vehicle offerings [1].

"Electrified vehicles" is an umbrella term used to define vehicles that make use of an electric propulsion system in their powertrain [2]. The main components that these systems are comprised of are a battery pack and an electric motor, and how these components are used in the powertrain varies depending on the vehicle's level of electrification. Electrified vehicles include mild hybrid electric vehicles (MHEVs), full hybrid electric vehicles (FHEVs), and full electric vehicles (EVs). The main distinction between these types of propulsion systems is in their reliance (or lack thereof) on an internal combustion engine (ICE) to propel the vehicle; MHEVs rely on an ICE as their main source of propulsion, FHEVs are capable of driving exclusively on electric power for a limited range before switching to an ICE, and EVs exclusively use electric power without any reliance on an ICE. Figure 1 summarizes the main differences between the configurations of electrified powertrains.

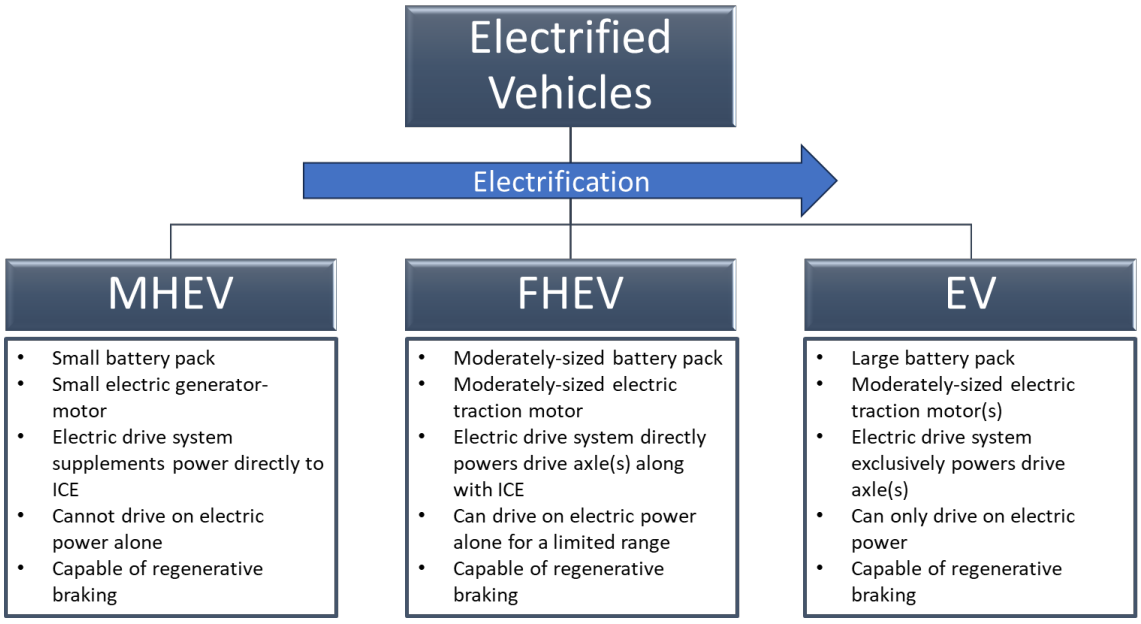

Figure 1. Diagram of vehicle electrification levels. Based on information contained in [3].

Electrified vehicles have rapidly grown in global market share in recent years due to a combination of factors such as shifting consumer preferences towards sustainability and efficiency, heightened regulatory demands from government bodies, and increased commitment and investment from the automotive industry [4]. A meta-analysis of automotive market trends performed out of Aachen University suggests that 54.3 % of all new vehicles will be electrified by 2030 [5]. The projected dominance of the automotive market by electrified vehicles has led to a surge in research efforts focused on their design [6], thereby advancing the development and maturity of electrified vehicle technologies.

1.1.2 Regenerative Braking

The rise of electrified vehicles in the consumer automobile market has prompted automotive manufacturers to explore novel driving features and energy optimization techniques in order to take advantage of the electric drive system's intrinsic capabilities. One such capability is the

implementation of regenerative braking, which in contrast to ICE vehicles, allows for the recycling of kinetic energy that would otherwise be lost to mechanical braking devices during vehicle deceleration. Regenerative braking is achieved by using the resistive electromotive force of the electrified powertrain's electric motor(s) to slow down the vehicle while also generating current to charge the high voltage battery [7].

Regenerative braking is typically integrated within the electrified vehicle's conventional braking control strategy, whereby the brake pedal position is used to generate a braking torque request that is then split between regenerative and friction braking, respectively [8]. This combined use of the hydraulically-actuated friction brakes and the electromotive resistance of the motor to decelerate the vehicle is referred to as a hybrid braking system (HBS), which is illustrated in Figure 2.

However, automotive manufacturers are increasingly developing methods for the driver to engage regenerative braking independently of the brake pedal, hereby referred to as decoupled regenerative braking. Common methods include engaging regenerative braking by lifting off the accelerator pedal (hereby referred to as lift-off regenerative braking) or by pressing on a wheel-mounted paddle. The motivation behind developing these methods is that they allow for an easier and less intensive driving experience by reducing the frequency at which the driver's foot position must switch between the accelerator and brake pedals, thereby reducing driver fatigue and braking response time in emergency maneuvers [9][10].

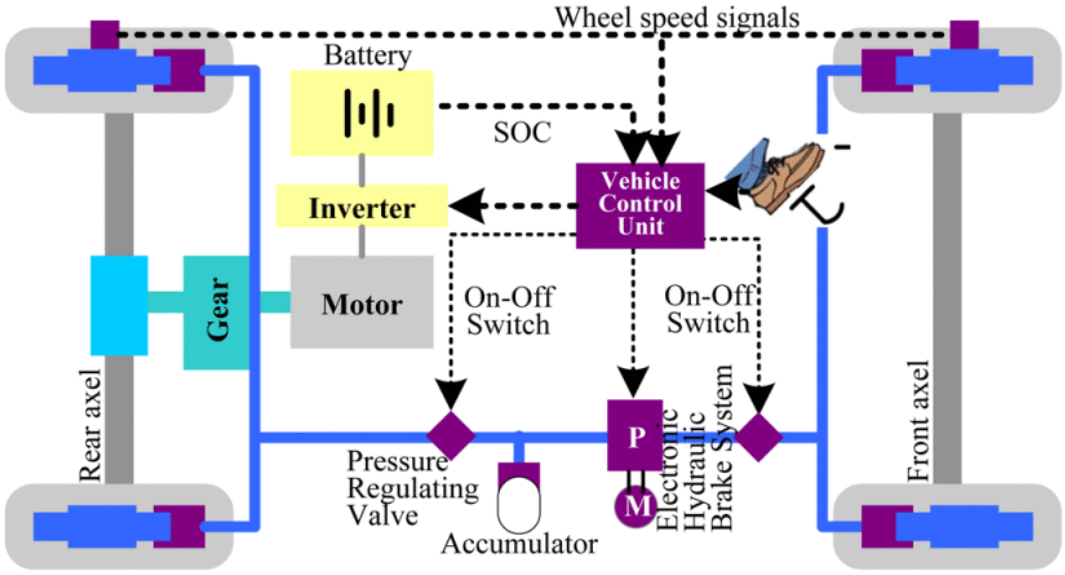

Figure 2. Hybrid braking system diagram. Reprinted from [9]. © 2016 IEEE

The level of braking force applied using either method of decoupled regenerative braking is a design variable [11]. As illustrated in Figure 3, a common implementation of decoupled regenerative braking involves demanding some constant negative torque value (i.e., the design variable) as soon as the driver engages lift-off or wheel-mounted paddle regenerative braking at normal driving speeds (greater than 5 m/s in this case). Depending on the car model, this design variable is either completely non-configurable (e.g., Tesla [12]) or can be changed via the driver selecting between different strength levels (e.g., Kia [13], Mercedes [14]). For example, the 2023 Nissan LEAF offers drivers the ability to select between a "D mode", which uses a low regenerative braking strength level to decelerate the vehicle at a similar rate to engine braking in an ICE vehicle, and a "B mode", which decelerates the vehicle more aggressively on accelerator pedal lift-off [15]. In some vehicles, the regenerative braking strength may also be indirectly changed by means of selecting different drive modes that are set to different strength levels [13].

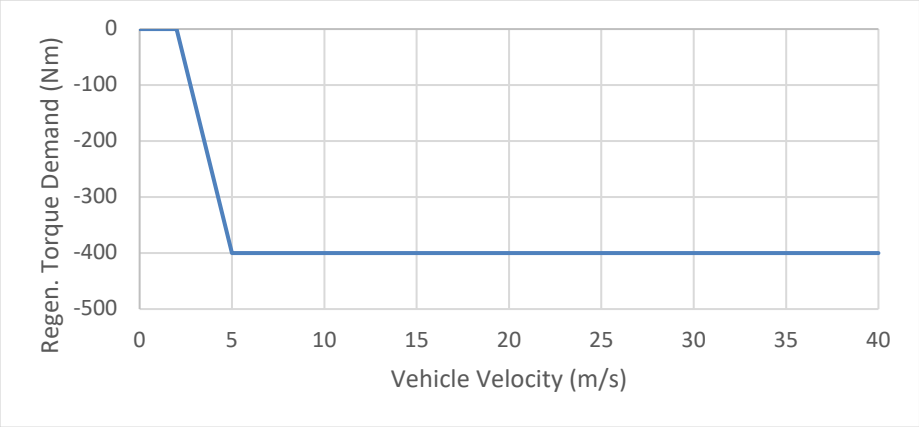

Figure 3. Example of lift-off regenerative braking torque as a function of vehicle velocity. Adapted from [16].

1.1.3 Drive Cycles

Drive cycles, which are profiles of vehicle speed over time, are collected from real-world travel routes or constructed by stitching together micro-trips [17]. These drive cycles are developed in order to mimic certain driving scenarios or driver behaviours for the purpose of analysing vehicle performance (e.g., emissions) across varying conditions [18]. The speed-time profiles of the drive cycles are heavily dependent on the routes that are selected to characterize a certain driving scenario. The actual driving conditions present throughout these routes often change, and variations in road

classification, speed limits, and traffic flow are reflected in different segments of the speed-time profile of a drive cycle [19]. The end result is a drive cycle that broadly represents a typical driving scenario or route (e.g., city driving) but contains periods of driving conditions that differ from one another.

The Urban Dynamometer Driving Schedule (UDDS) [20], which is used by the U.S. Environmental Protection Agency (EPA) to represent a city driving scenario, is a good example of a drive cycle with changing driving conditions. Figure 4 illustrates the speed-time profile of the UDDS, with periods of varying speed, acceleration, and stop frequency that are indicative of distinct driving conditions that change with time.

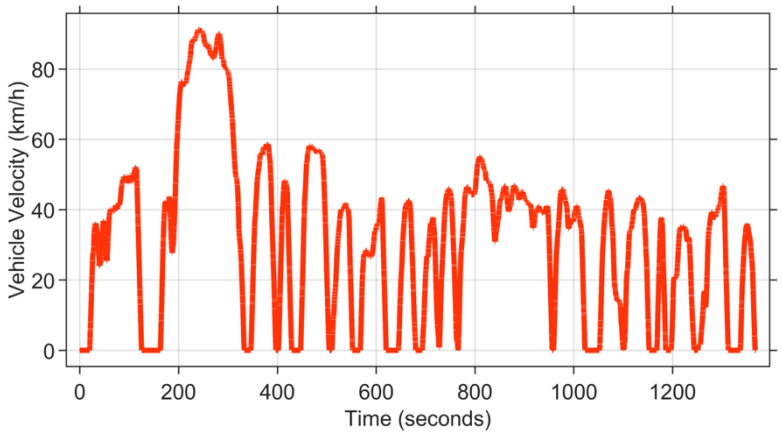

Figure 4. Speed-time profile of UDDS drive cycle. Adapted from [20].

Drive cycles fall into two principal categories: transient and modal [21]. Transient drive cycles simulate the dynamic nature of real-world driving, encompassing phases of acceleration, deceleration, and idling. In contrast, modal drive cycles are comprised of segments of steady-state driving with constant velocity or acceleration. The practical distinction between the two types of drive cycles is that transient cycles are collected from real-world driving data whereas modal cycles are not [22]. This key difference becomes apparent when comparing the transient UDDS cycle with the modal Japanese 10-15 (J1015) cycle in Figure 4 and Figure 5, respectively. The constant accelerations, decelerations, and velocity plateaus in the modal cycle are in stark contrast to the high degree of variation and stochasticity in the transient cycle, which is more representative of real-world driving.

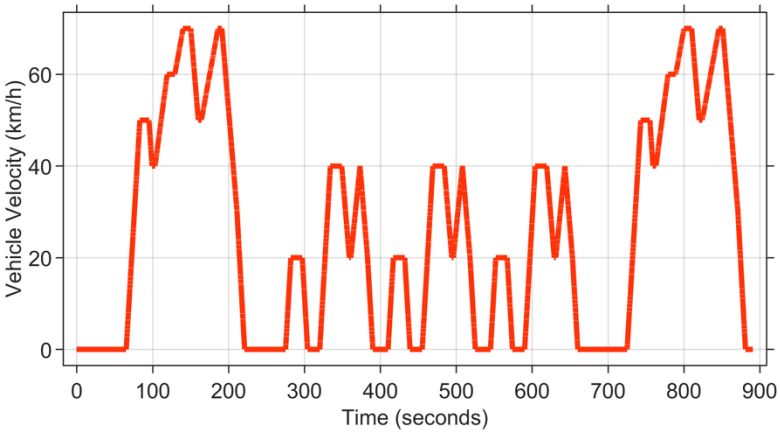

Figure 5. Speed-time profile of J1015 drive cycle.

1.1.4 Driving Conditions

Driving conditions are defined by a multitude of factors such as road classification, traffic congestion, weather, infrastructure, and topography [23]. Despite the breadth of these factors, driving conditions can largely be described by their road classification alone (e.g., urban, highway, etc.) [24][25][26]. They play a large role in dictating driver behaviour as well as the limits to which a vehicle can be driven, predominately impacting the vehicle's velocity and acceleration throughout a drive cycle [25].

It is well established that vehicle deceleration rates, whether by driver preference or environmental necessity, vary depending on the driving condition [27][28]. For example, Szumska and Jurecki found that the maximum deceleration during urban, suburban, and highway road drive cycles performed in the real world was 3.2 m/s^2, 3.0 m/s^2, and 2.6 m/s^2, respectively [29].

This variance in deceleration rate depending on driving condition has a subsequent impact on the effectiveness of regenerative braking systems. For example, even though the 2023 Kia Niro EV has four regenerative braking levels that the driver can choose from, the regenerative braking strategy is designed such that vehicle will actually decelerate less at higher speeds when compared to lower speeds despite being set to the same level [30]. In a study that experimented with varying levels of regenerative braking strength in urban driving conditions, it was found that energy consumption would actually start increasing at stronger levels beyond a certain point due to the driver having to intervene and correct excessive decelerations [31]. These findings suggest that there is no "one size fits all" setting for regenerative braking strength that can be used in all driving conditions.

1.2 Problem Identification

Decoupled regenerative braking systems implemented in electrified vehicles either use non-configurable design variables or rely on the driver to manually select their deceleration preferences among a limited list of options in order to dictate the negative torque that is requested from the electric drive system during regenerative braking. This reliance on infrequent (or non-existent) driver selections in order to prompt changes in the regenerative braking control strategy can lead to mismatched design variables that are not appropriate for:

- the driving environment in which the vehicle is operating
- the driver's deceleration preference.

For example, while having aggressive decoupled regenerative braking may be beneficial for reducing driver fatigue in urban driving conditions with frequent stops and strong decelerations, it is in fact detrimental to the driving experience in high-speed driving environments where the vehicle may decelerate beyond what is intended by the driver (e.g., coasting) [32]. This problem also has an implication on the driver's trust and acceptance of decoupled regenerative braking systems [33]. It follows that with lift-off regenerative braking systems (i.e., braking via releasing the accelerator pedal), a mismtached regenerative braking strength could lead to the driver having to manually adjust the pedals to counteract the undesirable deceleration rate. Having to frequently make these adjustments may be seen as an inconvenience for drivers. It would therefore be advantageous to the driving experience if the lift-off regenerative braking system of an electrified vehicle could learn a driver's preferred rate of deceleration for a given condition.

There exists a need for a sophisticated regenerative braking control scheme that can mitigate the occurrence of undesirable decelerations and promote a safer and more intuitive driving experience. This advanced system should possess the capability to not only reliably forecast the prevailing driving conditions with precision but also seamlessly adjust itself to harmonize with the driver's individualized preferences regarding regenerative braking strength.

1.3 Research Objectives and Contribution

Upon examination of the state of the art regarding decoupled regenerative braking systems, a noticeable practical challenge that has not yet been undertaken emerges: What novel approaches can be utilized to improve the driving experience of lift-off regenerative braking systems in electrified

vehicles? The research objective is thus to enhance the driving experience of lift-off regenerative braking systems by minimizing pedal usage during braking, thereby reducing driver fatigue and improving overall user comfort.

The research presented in this thesis addresses this objective by proposing a lift-off regenerative braking control scheme that adapts to the driver's preferences. In order to achieve this objective, the control scheme will need to:

- accurately identify current driving conditions to automatically change regenerative braking strength to an appropriate setting
- learn the driver's preferred lift-off regenerative braking deceleration such that pedal usage is minimized
- be compatible with automotive-standard embedded hardware running in real time.

The proposed solution that addresses these practical challenges is an adaptive regenerative braking controller that leverages the following innovative strategies:

- the novel application of the HDBSCAN clustering algorithm in order to identify distinct driving conditions in a comprehensive dataset of drive cycle intervals
- the use of a fuzzy inference system to achieve accurate online identifications of driving conditions in real time
- the novel application of the online Q-learning algorithm to find the optimal regenerative braking strength that minimizes an original cost function of pedal usage.

The introduction of advanced techniques such as HDBSCAN clustering, fuzzy inference, and online Q-learning as part of a driver-optimized lift-off regenerative braking control scheme marks a substantial contribution to the advancement and maturation of electrified vehicle powertrain control technologies.

Chapter 2
Literature Review

The research endeavor presented in this thesis is aimed at the development of an adaptive control system that learns a driver's prefered deceleration rate in different driving conditions. The ultimate objective of this control system is to minimize pedal usage during deceleration in an effort to improve the driving experience while using regenerative braking. This ambitious objective unfolds in two distinct domains: online driving condition identification and adaptive regenerative braking control. This section provides a comprehensive examination of previous research done in these two domains in order to highlight gaps in the literature.

2.1 Online Driving Condition Identification

Within the realm of online driving condition identification, the following areas of research are examined: Data Collection, Data Categorization, and Fuzzy Inference.

2.1.1 Data Collection

The development of an online identification scheme requires an understanding of the full range of possible driving conditions, which can be obtained by analysing vehicle data across a wide variety of realistic drive cycles. When it comes to selecting drive cycles for analysis, modal drive cycles are typically omitted from research that requires realistic driving data. Tong et al. explicitly omit modal cycles from their framework of drive cycle development as they do not characterize real driving behaviour [34]. Huzayyin et al. identify modal cycles and their unsuitability for representing the dynamics of driving on real-world routes as a primary motivation for their research into new drive cycle development [35]. In accordance with these findings, the research in this thesis will also omit modal drive cycles from its driving data collection process.

Since drive cycles are often composed of segments of driving conditions that are not necessarily consistent with each other, it is essential that these drive cycles be divided into intervals that capture the characteristic driving conditions throughout the drive cycle with greater granularity. A common approach to segmenting vehicle data into intervals is to use vehicle stand-still phases to separate individual micro-trips (MTs) [36][37]. Förster et al. define MTs as a vehicle stand-still phase followed by a driving sequence until the next vehicle stand-still phase [38]. Since very short MTs

collected in stop-and-go conditions lack representativeness, in their research they merge adjacent MTs until a minimum duration is reached. This method is problematic since basing the intervals on stand-still phases means that valuable information regarding the number of stops during a driving sequence is lost (excluding the edge case where short MTs are merged). Alternatively, Hu et al. divide driving segments by time elapsed, using a fixed step size of 100 seconds [39]. While basing the driving intervals on time elapsed preserves information regarding the number of stops, this method can easily be skewed by long periods of stand-still phases. For example, segments 1, 4, and 5 of the New York City Cycle (NYCC) in Figure 6 will have metrics related to velocity and acceleration skewed towards zero due to their long periods of idle time. To avoid these drawbacks, this thesis proposes a method for segmenting drive cycles by distance traveled, thereby preserving information related to the number of stops within a segment while avoiding the limitation of having prolonged stop times skew the data.

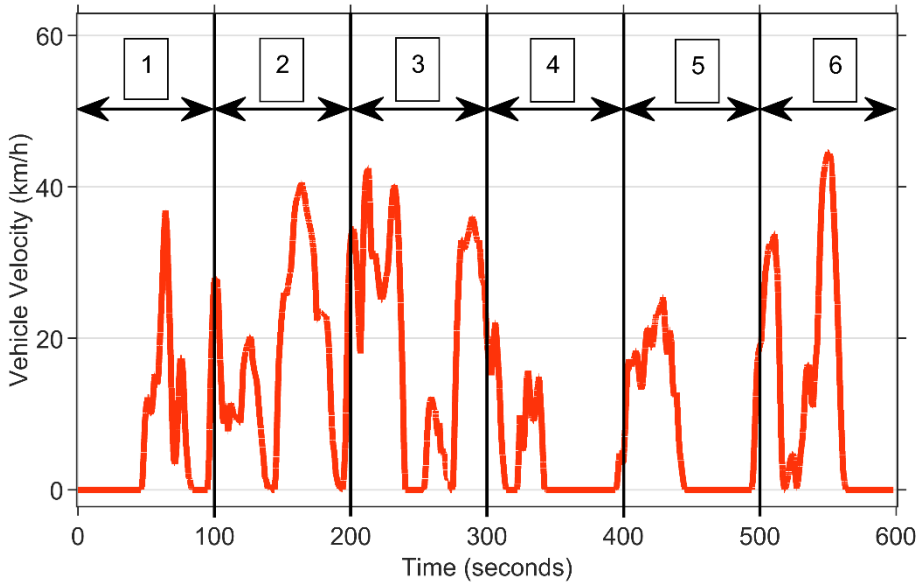

Figure 6. Division of NYCC into six driving segments by time-elapsed. Adapted from [37].

2.1.2 Data Categorization

A common method of categorizing intervals of vehicle data is to differentiate them based on predefined value ranges. Value range determination through domain knowledge is a manual approach where experts or analysts leverage their expertise in the relevant field to establish predefined intervals

or cutoff points for data values. For example, Lee et al. categorize drive cycles based on whether the distance traveled is less than 9 miles, greater than 9 miles but less than 20 miles, or greater than 20 miles [40]. In a similar approach, Shahidinenjad et al. categorize drive cycle MTs using manually-selected value ranges that describe low, moderate, and high average speed and mild, moderate, and harsh acceleration [41]. Since value ranges are typically defined based on human judgement or domain knowledge, using this approach can introduce bias or overlook important data patterns if the value ranges lack granularity. Furthermore, driving conditions are often too complex to be inferred from individual vehicle data signals alone and are better characterized by the analysis of multiple interrelated signals whose direct relationships to the driving condition are not well defined [38]. Therefore, the value range method is limited in its ability to accurately capture the full spectrum of vehicle data that characterizes different driving conditions. It is thus desirable that the online driving condition identification scheme is capable of accurately finding relationships between collected data signals that may not be explicitly defined.

The task of exploring hidden relationships in a complex dataset is well suited for unsupervised machine learning algorithms. The application of unsupervised clustering algorithms for the purpose of grouping data in complex datasets is well established in the literature [42]. Förster et al. applied unsupervised clustering to group drive cycle intervals into pre-defined classifications for the purpose of creating new drive cycles [38]. Hou et al. also used a clustering model to separate entire drive cycles into three representative groups that were pre-determined based on foreknowledge [43]. Likewise, Hu et al. decided to use a fixed number of clusters to identify different classes of driving conditions, selecting three clusters based on a qualitative assessment of the distribution of mean feature values in each class [39]. This represents one of the major limitations of these studies, in that they pre-define the number of clusters that represent the full range of characteristic driving conditions using foreknowledge or via a trial-and-error process of visually inspecting the clusters until there is enough distinction between them. These methods introduce a bias in the cluster identification process and negate one of the primary strengths of cluster analysis which is to aid in identifying unforeseen relationships in data (i.e., data exploration) [44]. To mitigate the influence of bias when determining the number of clusters that exist within the dataset, the work in this paper will follow a systematic approach using the Elbow Method [45].

The previously discussed research regarding the clustering of drive cycles employed some form of the K-means clustering algorithm, which is among the most popular clustering algorithms in use [46].

The algorithm works by partitioning the dataset into clusters by minimizing the sum of squared distances between data points and their corresponding cluster centroids [47]. One of the limitations of the K-means algorithm is that since it partitions the entire dataset assuming spherical data clusters of similar shape and density, it performs poorly in many real-world datasets that contain regions of varying density, arbitrary cluster shapes, and noise [48]. The K-means algorithm assumes that there is no noise and that there are exactly *K* number of clusters in the data, where *K* is a hyper-parameter that is selected using foreknowledge of the dataset. This is especially problematic in the data exploration task of the drive cycle interval dataset since little is known about the underlying driving condition clusters within. It is therefore advantageous to instead consider a clustering method that makes fewer assumptions about the underlying distribution of data and is thus more suitable for real-world datasets.

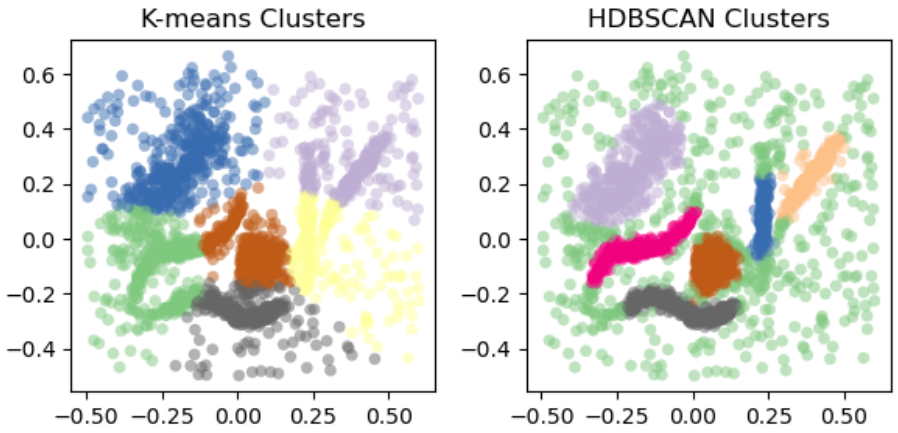

Figure 7. Comparison of clusters identified by HDBSCAN and K-means models fitted to a dataset [49] with irregularly-shaped clusters and noise. Clusters are distinguished by colour.

As opposed to K-means, the Hierarchical Density-Based Spatial Clustering of Applications with Noise (HDBSCAN) algorithm uses a density-based approach to identify a cluster hierarchy within a dataset [50]. This allows HDBSCAN to identify clusters of irregular shapes and sizes while discarding noise. Figure 7 illustrates how HDBSCAN identifies more representative clusters in a dataset [49] with irregularly shaped clusters and noise when compared with K-means. Unlike K-Means, HDBSCAN does not require any assumptions to be made about the number of clusters within a dataset. These qualities lend themselves well to the clustering of vehicle data collected across numerous drive cycles, since we cannot conclusively know how many driving conditions exist in the

data *a priori.* Furthermore, the collection of multiple telemetry signals results in a dataset of high-dimensionality and an increased potential for noise, which the HDBSCAN algorithm is better suited to handle [48]. For these reasons, the research presented in this thesis will use the HDBSCAN algorithm to cluster drive cycle intervals.

The HDBSCAN clustering algorithm has seen limited use in automotive applications. Previous works have applied its predecessor, DBSCAN, for data exploration related to driver behavior. Zhang et al. used DBSCAN on a dataset of vehicle trajectories to label drivers based on their driving style [51], while Wang et al. used it to find clusters of driving behavior based on recorded driving events (e.g., speeding, sudden braking, etc.) [52]. DBSCAN has also been used to identify idle conditions in a vehicle telemetry dataset collected during drive cycle simulations [53]. However, to the author's knowledge, neither the HDBSCAN nor the DBSCAN algorithms have been used to identify the underlying driving conditions in a dataset of drive cycle intervals. Thus, this paper proposes a novel application of HDBSCAN.

2.1.3 Online Identification

Many of the previously discussed works are solely interested in offline clustering and system identification schemes. When it comes to online identification schemes, previous studies have mainly focused on identifying driver behavior rather than driving conditions [50][54]. Regarding driving condition identification, Hu et al. proposed a scheme that identified classes of driving conditions by calculating the Euclidian distance between the features of the most recently recorded data interval and the centroid of the class [39]. However, the distance associated with each feature was not weighted or otherwise scaled for unit variance, meaning that the class identification scheme in this study was dominated by the Euclidian distance of the feature with the largest units (i.e., velocity). Therein lies one of the main limitations of this method, in that outliers in the data due to noise or improper scaling can easily skew the distance measurement towards an erroneous identification. Another limitation of the Euclidian distance method for online identifications is that it is incapable of considering the joint influence of variables in multidimensional data (e.g., the interrelation between velocity, acceleration, etc. in a driving interval). Hou et al. proposed a driving condition identification scheme that used a Support Vector Machine (SVM) learning model to make online classifications of recently recorded vehicle data intervals in a simulation environment [43]. However, the demanding computational requirements of an SVM model as a result of needing to process a large number of support vectors

means that it is not well suited for embedded applications, such as in vehicle controller hardware [55]. For this research, an online identification method that can handle noisy, multidimensional data and is compatible with embedded vehicle controller hardware is required.

Fuzzy logic is a powerful tool for dealing with complex systems where inputs and outputs are not always explicitly defined, and it is well suited for applications that require a more flexible and nuanced representation of uncertainty in data [56]. Since driving conditions are somewhat vague and are not explicitly defined by absolute numerical values, fuzzy logic is well suited for the process of identifying them by using rules and membership functions that determine a degree of belongingness to a certain condition. Fuzzy logic systems have been extensively researched in embedded automotive applications such as in anti-lock braking, adaptive automatic transmission, and engine control [57]. When it comes to making online identifications of driving conditions, Schüler et al. used existing experience to determine the membership functions for mean throttle velocity, mean throttle angle, longitudinal acceleration, and mean speed to identify traffic jam, city, road, and highway conditions [58]. Zhang et al. used fuzzy logic to classify driving patterns based on average speed and maximum speed, once again manually determining the value ranges of the membership functions based on prior experience [59]. While the use of prior knowledge to design a fuzzy logic system is necessary for designing meaningful rules, it nonetheless introduces an element of bias, especially when designing membership functions that are based on foreknowledge rather than data.

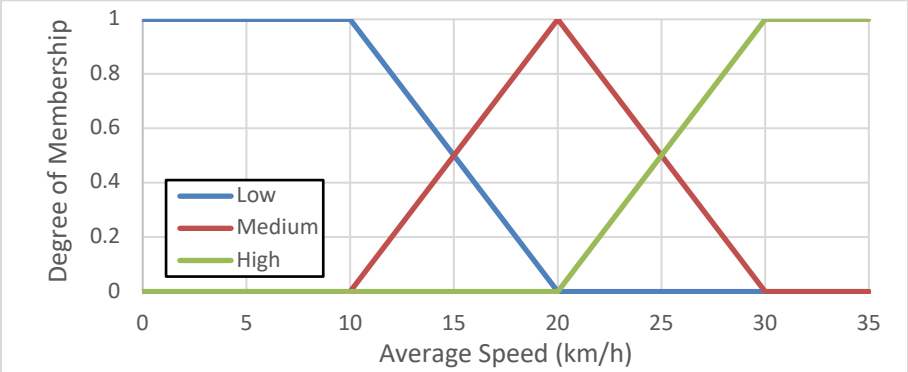

Figure 8. Example of membership functions for three driving patterns used in a fuzzy logic system. Adapted from [59].

Take the membership functions used by Zhang et al. for example. The average speed membership functions for the fuzzy sets of low, medium, and high speed driving patterns are illustrated in

Figure 8. The “medium” average speed membership function is precisely centered on 20 km/h. However, since driving conditions are ambiguous, how can we know for certain that this is exactly the value that signifies “medium” driving conditions the best? This is where the advantages of data-driven clustering come into play, whereby the membership functions can be made to be more representative by centering them on the cluster centroids. In order to preserve the incorporation of expert knowledge while also taking advantage of the pattern recognition capabilities of data-driven clustering, this research proposes a cluster-informed fuzzy inference system to achieve the online identifications of driving conditions.

2.2 Adaptive Regenerative Braking Control

The domain of adaptive regenerative braking control is divided into the following research topics: Driver Preferences, Regenerative Braking Control, and Adaptive Control.

2.2.1 Driver Preferences

The justification for this research into adaptive regenerative braking relies on the assumption that different drivers have different deceleration preferences. In a study of driving style preferences conducted in a high-fidelity simulator, 72 participants were subjected to different variations of lane change, acceleration, and deceleration maneuvers, respectively, and asked to select their preferred variation [60]. The deceleration maneuver ended up having the greatest overlap in preference score between competing variations, indicating that participants were split regarding which deceleration profile they preferred. In their research involving personalizing the acceleration and braking behaviour of a vehicle’s advanced driver assistance system (ADAS), Vadim and Ioannou collected vehicle data from 3 drivers doing test drives in an urban area and found that in contrast to the observed acceleration behaviours, there was no uniformity in the deceleration behaviours between the drivers [61]. These findings suggest that deceleration preferences between drivers differ significantly and that it is therefore advantageous to adapt the deceleration characteristics of the vehicle to an individual driver.

Another important assumption that forms the basis of this research is that drivers’ preferred deceleration changes depending on the driving condition. In a study of the acceleration behaviour of 24 participants driving on a route containing extra-urban roadways, arterial roads, and motorways, Bosetti et al. found that drivers were more likely to decelerate more aggressively on roads with high

curvatures (associated with urban conditions) when compared with low-curvature roads (associated with highway conditions) [62]. This is corroborated in Yavas et al.'s analysis of a real-world highway driving dataset, which found that drivers prefer coasting over braking while approaching slower vehicles [63]. Wortman and Fox discovered that when drivers approach signalized intersections, their deceleration pattern is mainly influenced by their initial approach speed [64]. This suggests that under different driving conditions and travel speeds, drivers would have distinct preferences for how quickly they prefer to decelerate. To elaborate further, Wallace et al. conducted a year-long study on the driving behavior of an older subject and observed that the rate of deceleration was significantly affected by the *change* in velocity during a deceleration event [65]. Figure 9 illustrates the relation between deceleration and velocity change using recorded data from nearly 25,000 braking events, showing deceleration rates increase as the velocity change increases until an asymptote is reached (at approximately -2 m/s^2 in this case). When we consider this in the context of driving conditions, it logically makes sense that subtle adjustments to a vehicle's speed on a highway would be done at a lower deceleration, whereas reacting to a moving obstacle (e.g., other vehicles, pedestrians) or approaching an intersection in an urban or arterial environment would require larger decelerations.

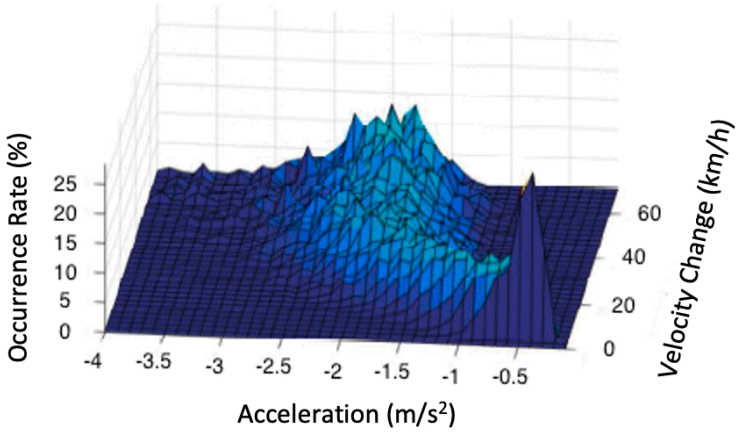

Figure 9. Distribution of minimum acceleration against velocity change across all recorded deceleration events. Reprinted from [65]. © 2015 IEEE

Other studies have shown that deceleration preferences are not dictated by the vehicle's travel velocity alone. In his study of driver acceleration behaviours on Canadian roads, Yang found that the deceleration profiles with respect to speed differed depending on whether the road was a highway or urban road [66]. For example, at speeds greater than 90 km/h the mean deceleration rate on urban

roads was up to 173 % greater than those on highways at the same speed. In his review of previous research conducted on deceleration behaviours, Deligianni identified the following relevant factors as having significant effects on a driver's preferred deceleration rate: traffic conditions, speed, time to collision, and headway [67]. These are all factors that are significantly influenced by driving conditions [68].

Regenerative braking presents a learning curve for drivers as they need to adjust their braking techniques and learn to anticipate its unique braking response for comfortable deceleration. In terms of the implementation of decoupled regenerative braking systems, drivers generally prefer systems triggered by the accelerator pedal (i.e., lift-off regenerative braking) as opposed to one triggered by the brakes [69]. When it comes to the strength of regenerative braking, studies seem to indicate that driver preferences are mixed. In their 1-year field study on driver interactions with regenerative braking systems, Cocron et al. found that while acceptance of the lift-off regenerative braking system was high, drivers found it more useful than satisfying [33]. Some drivers had difficulties adapting to the system, with some complaining that the deceleration rate was too strong, that it led to frequent early stops, and that it prevented the ability to coast. This is in contrast to another study in which test drivers reported less discomfort at higher rates of regenerative deceleration [70]. These studies reveal significant variation in driver preferences regarding regenerative braking strength. Therefore, it is evident that researching methods to enhance driver satisfaction while using the system is a valuable pursuit.

2.2.2 Regenerative Braking Control

Since lift-off regenerative braking is governed by the calculation of deceleration torque to request from the vehicle's electric motor(s) (i.e., a single design variable), several studies have been conducted in order to optimize this torque request. The vast majority of these studies involve the development of control strategies the maximize the energy recuperated during braking. Kim et al. proposed a deceleration planning system for connected and automated vehicles (CAVs) in which an energy-optimized deceleration rate is calculated based on map-based geographic information and connectivity-based traffic signal information [71]. For the deceleration planning system to work, measurements of final speed, remaining braking distance, and remaining braking time are required. This limits the application of such a system to deceleration events that exclusively occur before vehicle-to-everything (V2X) communication-capable intersections where accurate geographic data is

also available. Furthermore, because the system attempts to maximize the energy recovered during deceleration, it ends up selecting the most aggressive deceleration in every case (see Figure 10), since that is what generates the most electric current for battery charging. In some cases, the deceleration rates selected by the system were as high as 10.08 m/s^2, which is 152 % greater than the threshold at which drivers begin feeling significant discomfort (4 m/s^2) [72][73]. This suggests that systems that are designed to exclusively optimize energy recuperation during deceleration are likely to worsen driver comfort and satisfaction.

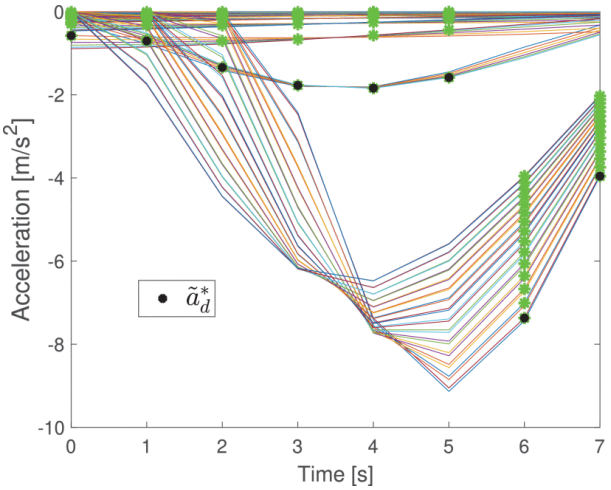

Figure 10. Optimal decelerations (black circles) selected from possible deceleration candidates (green asterisks) based on a set of deceleration profiles (colourful lines) for two different deceleration paths. Reprinted from [71].

In their study comparing regenerative braking strategies for decelerating to a complete stop, Chakraborty and Nandi designed a regenerative braking controller that optimized two objectives during a deceleration event: the maximization of recuperated energy and the minimization of the duration of deceleration [74]. In their study, they conducted a comparison between employing a constant negative torque request and employing a dynamic torque request during deceleration. This comparison was conducted while imposing different limits on the maximum allowable jerk, which refers to the rate of change of deceleration. As expected, having no constraints on the maximum allowable jerk resulted in the greatest energy recovered for both approaches. However, the jerk values sustained during these decelerations were as high as 18 m/s^3, which is 350 % higher than the 4 m/s^3 threshold at which drivers begin to feel uncomfortable [72][73]. The tendency in the literature to

prioritize energy efficiency over driver comfort when designing regenerative braking controllers is evident in this oversight of the user experience. At the lowest studied jerk constraint of 7 m/s^3 (which is still significantly greater than the threshold of discomfort), a constant deceleration rate resulted in greater energy recovered. Since there does not seem to be a benefit to complicating the control of regenerative braking with multiple stages of deceleration, the adaptive control scheme presented in this research will use a constant deceleration rate during lift-off regenerative braking.

Dehkordi et al. developed an energy-optimized control scheme that would maximize the use of regenerative braking as opposed to hydraulic braking for a given velocity profile [75]. Similar to Kim et al.'s research, the effectiveness of this control scheme faces limitations because it relies on knowing the final steady-state velocity to determine the velocity profile. This approach is valuable for applications of ADAS on highways like adaptive cruise control (ACC), where velocity predictions are more reliable. However, in dynamic and unpredictable urban driving scenarios, estimating final steady-state velocities becomes considerably more challenging. A notable aspect of Dehkordi et al.'s work is that, despite primarily focusing on energy recovery optimization, they also incorporated user-oriented control constraints. This demonstrates their commitment to considering driver satisfaction and comfort in their research. Instead of controlling braking torque, they employed acceleration as the control variable for their regenerative braking controller. This choice enabled them to set a control constraint directly, limiting unsafe and uncomfortable deceleration to 4 m/s^2, which aligns with the previously stated threshold of discomfort. Additionally, the selection of deceleration as the control variable makes their controller more modular and adaptable to a wide range of electrified vehicles since unlike torque, deceleration does not depend on vehicle-specific factors like curb mass and electric motor selection. As a result, the adaptive regenerative braking controller presented in this thesis will also use acceleration as its control variable.

2.2.3 Adaptive Control

Prior research has been conducted on automatically adapting various aspects of vehicle control to the detected driving conditions. This is often achieved by categorizing a recorded driving interval then choosing a suitable control parameter value that aligns with the identified driving condition. In their development of an adaptive energy management strategy for a FHEV, Lin and Li employ a real-time system that identifies one of four driving conditions and selects the appropriate power distribution strategy accordingly [76]. These strategies are predetermined through offline optimization

conducted on a single representative drive cycle for each driving condition (urban, sub-arterial, arterial, and freeway). However, it is important to note that a significant limitation of this approach is that optimizing control parameters for a single drive cycle lacks generality and can result in an "over-fitting" scenario, where the control parameters are well-suited for one specific drive cycle rather than being adaptable to multiple drive cycles or driving patterns with similar conditions.

Another approach to adaptive vehicle control is to categorize drivers based on their behavior and then choosing a suitable control parameter to match. Huang et al. classified drivers as “Aggressive”, “Ordinary” or “Cautious” in real time and used the classification to select among predefined values for maximum braking deceleration in an ACC system [77]. Their research concluded that this approach improved driver adaptability and comfort, suggesting that a similar adaptation of the deceleration rate in a regenerative braking system could yield promising results.

In Kubaisi's research on developing an adaptive regenerative braking strategy, he employed driver behavior categories and driver intention estimation to determine an appropriate braking torque [78]. The strategy was designed to use driver behaviour classification for selecting the right braking torque from a predefined set of values, each associated with a specific driver intention (such as driving, cruising, or braking). However, this approach has limitations as it lacks personalization for individual drivers, relies on seemingly arbitrarily predetermined deceleration values for each driver behaviour-intention combination, and does not clearly explain how driver intention affects the desired deceleration rate, especially since the relevant intention, normal braking, can be easily measured through pedal positions. One fundamental issue in Kubaisi's research is the choice of torque as a control variable instead of deceleration. Kubaisi attempted to relate torque and deceleration using a formula derived from empirical simulation data collected during deceleration events on a flat road surface. This approach overlooks the significant influence of road gradient on a vehicle's acceleration (e.g., a vehicle going uphill may decelerate even without applying braking torque). In contrast, this thesis will utilize deceleration as the primary control variable and leverage well-established automotive dynamic equations to determine the necessary braking torque. Additionally, the adaptive control scheme introduced in this work will learn from each individual driver's preferences and behaviour, ensuring a personalized approach to adaptive regenerative braking.

In his research, Nelles developed an adaptive gear shift strategy for automatic transmissions that learns from the driver in order to individualize the system’s shift behaviour [79]. This was achieved

by analyzing recorded vehicle data through a fuzzy inference system, categorizing drivers as either "Eco" or "Sporty" to varying degrees. Notably, Nelles introduced the concept of driver interventions to guide the learning process; when a driver manually changed gears, it triggered an update of the weights associated with a fuzzy set. Building on this approach, the research presented in this thesis will incorporate a novel cost function that considers driver intervention during lift-off regenerative braking in order to guide the learning process.

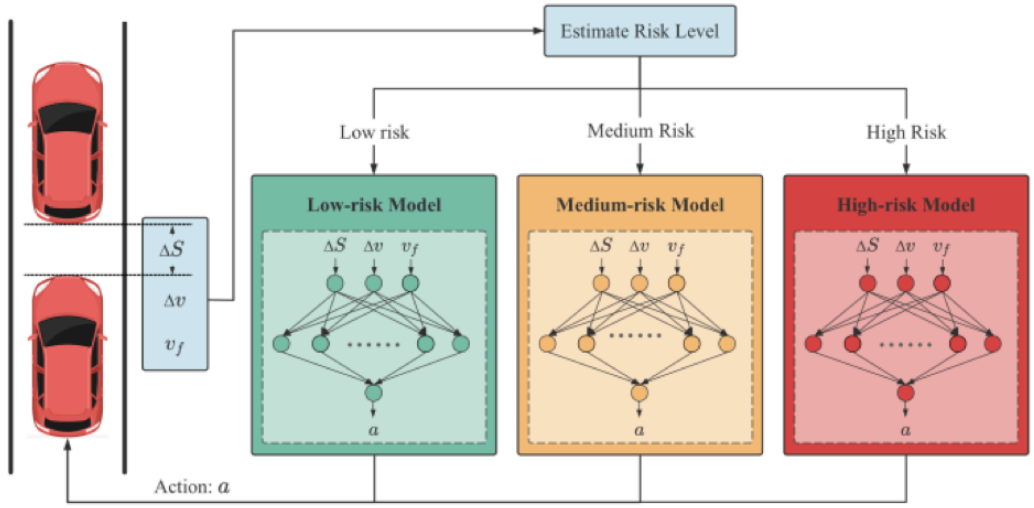

Figure 11. Adaptive vehicle trajectory control algorithms for different risk levels. Reprinted from [80]. © 2023 IEEE

In a study by He et al., reinforcement learning was used to adapt a car-following trajectory control algorithm to different levels of perceived risk [80]. They employed the Deep Q-learning algorithm [81] to learn separate policies for controlling the speed of the vehicle during ACC operation, each tailored to a specific risk level. To guide the Q-learning agent's learning process, they designed a reward function that penalized the agent based on a collision risk score, calculated in real-time based on factors such as relative velocity and following distance. This allowed the Q-learning agent to learn the appropriate car following trajectory for each risk level. During actual vehicle operation, their control system employed an adaptive switching strategy to select the appropriate trajectory control parameters based on the currently perceived risk level (refer to Figure 11). Notably, their adaptive algorithm significantly reduced jerk compared to human drivers, leading to improved driver comfort. In a similar approach to He et al.'s work, the work presented in this thesis will utilize Q-learning to

independently learn the optimal deceleration for various driving conditions. An adaptive switching strategy will be implemented to select and continuously update the optimal deceleration based on the detected driving conditions.

Chapter 3
Methodology

The following section will discuss the methodology that was used to develop and test the proposed adaptive regenerative braking control scheme. Firstly, the models that were used for simulation throughout development will be discussed. Following this, the methodology for designing the control scheme itself is subdivided into the distinct domains of online driving condition identification and adaptive regenerative braking control. Figure 12 illustrates a flowchart of the resulting adaptive regenerative braking control process. Finally, the simulation and experimental testing methodology will be discussed.

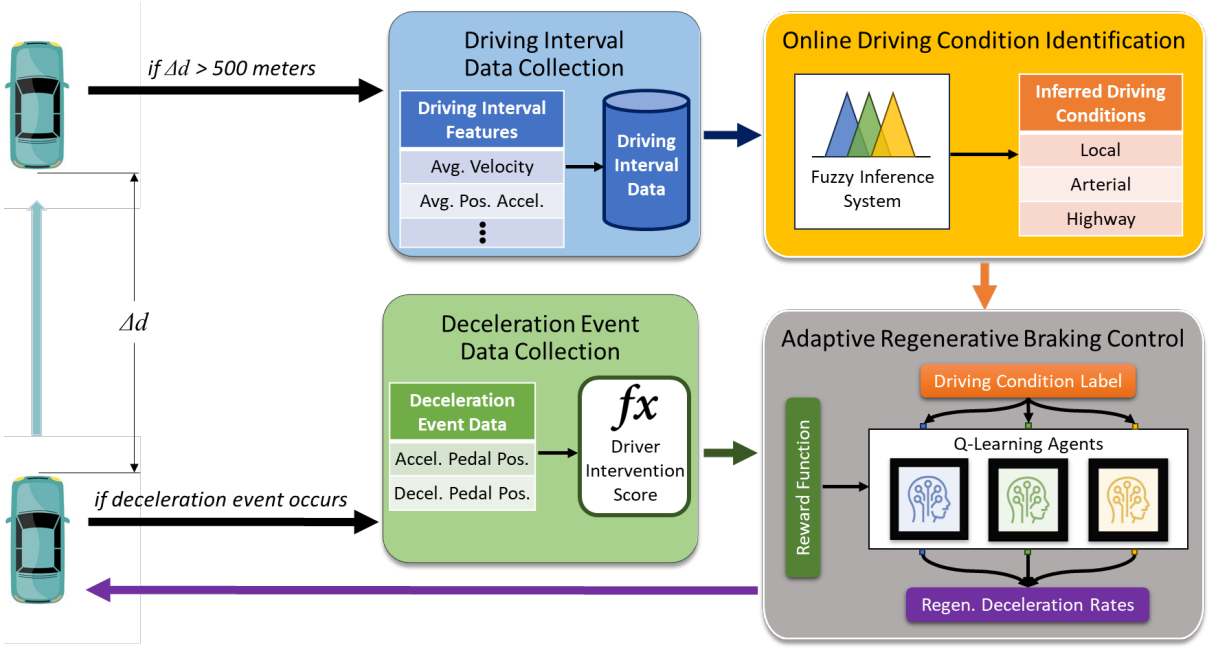

Figure 12. System flowchart for adaptive regenerative braking control system.

3.1 Modeling

In order to collect data for clustering as well as to test the adaptive control scheme in simulation, a model of an electrified vehicle is created in a MATLAB/Simulink environment. This section will provide a high-level overview of the key components of the vehicle model that are relevant in the context of lift-off regenerative braking. Essentially, the model encompasses mathematical depictions of the vehicle's dynamics (referred to as the plant model) and control algorithms that govern the

vehicle's operations (referred to as the controller model). To maintain conciseness, modeling aspects that are not explicitly related to regenerative braking are omitted from this section. This includes tire modeling, friction brake modeling, and battery management, among others.

3.1.1 Vehicle Body

This research requires the simulation of drive cycles. Since drive cycles solely represent a vehicle's longitudinal motion, the vehicle body only needs to be modeled with 1 degree of freedom in the longitudinal direction. The vehicle's dynamics are thus described by a rigid vehicle body of constant mass undergoing longitudinal motion. The model includes the influence of both inertial and drag loads to ensure an accurate representation of the vehicle's behavior during deceleration.

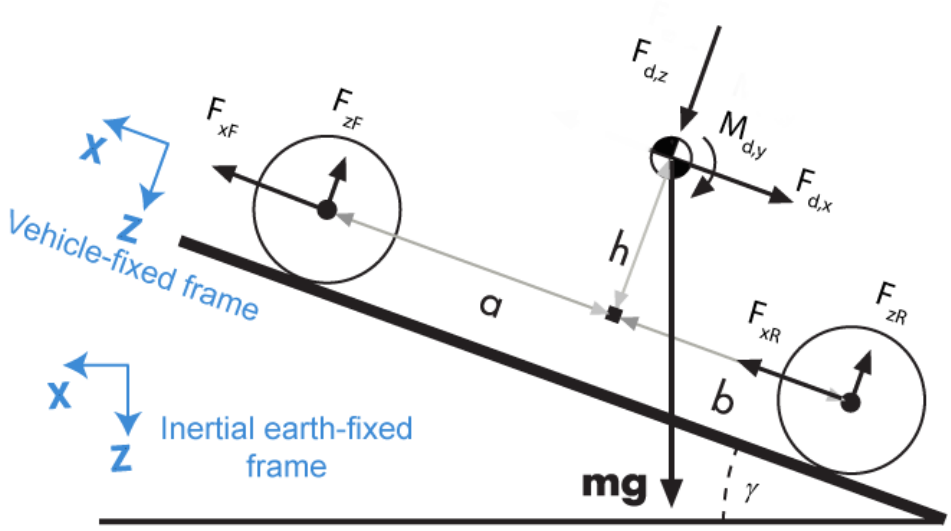

Figure 13. Free body diagram of longitudinal vehicle body model. Adapted from [81].

The vehicle body model consists of two parallel axles forming a flat plane, as illustrated in Figure 13. The equations of motion for the longitudinal vehicle model are as follows:

$$F_{xF} + F_{xR} - F_{d,x} - m\,g\sin\gamma = m\ddot{x} \tag{1}$$

where F_{xF} and F_{xR} represent the longitudinal forces on the wheels at the front and rear ground contact points, respectively, $F_{d,x}$ represents the longitudinal drag force, m is the vehicle body mass, g is gravitational acceleration, and γ is the angle of the road grade.

The normal forces acting on the front and rear axle wheels (assuming two wheels per axle) are given by the following equations:

$$2F_{zF} + 2F_{zR} = m\ g \cos\gamma \tag{2}$$

$$F_{zF} = \frac{-M_{d,y} + b\left(F_{d,z} + m\ g\cos\gamma\right) - h\left(F_{d,x} + m\ g\sin\gamma + m\ddot{x}\right)}{2(a+b)} \tag{3}$$

$$F_{zR} = \frac{-M_{d,y} + a\left(F_{d,z} + m\ g\cos\gamma\right) + h\left(F_{d,x} + m\ g\sin\gamma + m\ddot{x}\right)}{2(a+b)} \tag{4}$$

where F_{zF} and F_{zR} are the normal forces acting on each front and rear wheel, respectively, $M_{d,y}$ is the moment due to drag about the vehicle body's y-axis, a and b are the distance between the center of gravity and the front and rear axles, respectively, and h is the height of the center of gravity above the axle plane.

The drag forces acting on the vehicle body are solely comprised of aerodynamic drag. Assuming no wind speed, the drag forces and moments acting on the vehicle are given below:

$$F_{d,x} = \frac{1}{2}\rho\ C_d\ A_f\ \dot{x}^2 \tag{5}$$

$$F_{d,z} = \frac{1}{2}\rho\ C_l\ A_f\ \dot{x}^2 \tag{6}$$

$$M_{d,y} = \frac{1}{2}\rho\ C_{pm}\ A_f\ \dot{x}^2(a+b) \tag{7}$$

where ρ is air density, C_d is the drag coefficient, C_l is the lift coefficient, C_{pm} is the pitching moment coefficient, and A_f is the frontal area of the vehicle body.

3.1.2 Powertrain

The vehicle model features a fully electric rear-wheel-drive powertrain with a single electric motor. The electric motor dynamics are represented by a mapped model consisting of look-up tables of known motor parameters. The model receives a torque request from the torque controller as an input and uses tabulated loss data to determine the power loss associated with the requested torque at the current motor speed. These tabulated losses are given by a 2-dimensional look-up table relating efficiency to torque and speed, as illustrated in Figure 14. The current required to satisfy the torque request is then calculated as follows:

$$I_m = \frac{P_{req} + P_{loss}}{V_{bat}} = \frac{\omega_m T_m + (1 - \eta_m)\,\omega_m T_m}{V_{bat}} \tag{8}$$

where I_m is the current passing through the motor, V_{bat} is the battery voltage, ω_m is the motor speed, T_m is the motor torque, and η_m is the motor efficiency. Since this research is focused on regenerative braking, it is important to note that these dynamics are also valid for *negative* motor torque.

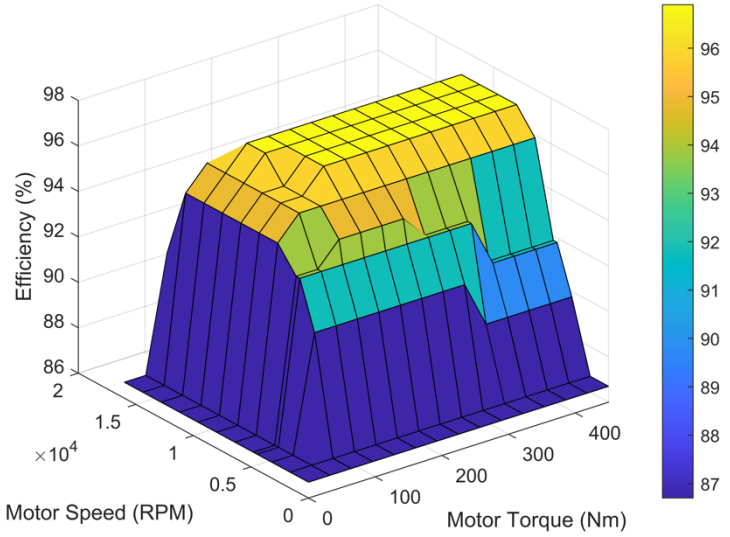

Figure 14. Example of a 2D look-up table relating motor efficiency to torque and speed.

Likewise, the battery model representing a lithium-ion battery pack is also parametrized by look-up tables created from manufacturer datasheets. This includes parameters such as open-circuit voltage, internal resistance, and number of cells. Battery voltage is calculated using the following equations:

$$V_T = E_m - I_{bat}\, R_{int} \tag{9}$$

$$I_{bat} = \frac{I_m}{N_p} \tag{10}$$

$$V_{bat} = N_s\, V_T \tag{11}$$

where V_T is the voltage per battery module, E_m is the battery's open-circuit voltage, I_{bat} is the current per battery module, R_{int} is the internal resistance, N_p is the number of cells in parallel, N_s is the number of cells in series, and V_{bat} is the battery pack voltage.

3.1.3 Torque Control

The torque controller interprets the driver's commands to establish the torque request delivered to the electric motor. This request adheres to the limits set by the manufacturer for the motor, as determined by a torque-speed envelope that defines the maximum power output of the motor at varying speeds (refer to Figure 15). The driver's commands are provided through the accelerator and brake pedals in order to request positive or negative torque to the electric motor, respectively.

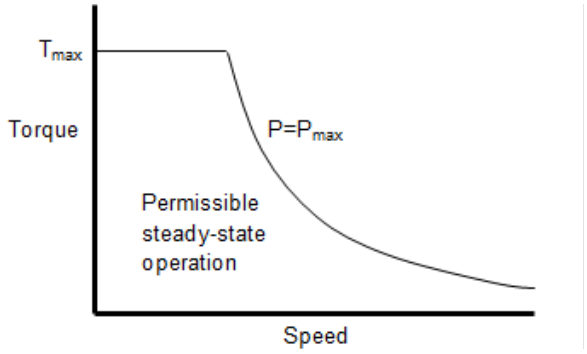

Figure 15. Generic torque-speed envelope for determining maximum motor power at a given speed. Reprinted from [82].

When the driver actuates the accelerator pedal, a linear pedal mapping is used to convert accelerator pedal position into a torque request. Torque is calculated by simply taking the accelerator pedal position and multiplying it by the maximum available motor torque at the current motor speed. To allow for coasting, pedal positions less than or equal to 1 % do not result in a torque request, as shown in the following equation:

$$T_m = \begin{cases} 0, & APP \leq 1 \\ APP * T_{max}, & APP > 1 \end{cases} \tag{12}$$

where APP is the accelerator pedal position given as a percentage and T_{max} is the maximum available motor torque.

When the brake pedal is engaged, the torque controller computes a braking pressure request that corresponds to the position of the pedal. The braking pressure is calculated as follows:

$$P_{brk} = BPP * P_{max} \tag{13}$$

where BPP is the brake pedal position given as a percentage and P_{max} is the maximum line pressure of the hydraulic braking system. This braking pressure request is transferred to a braking controller,

which transforms it into a braking torque request, considering the characteristics of the disc brakes. The controller divides the overall braking torque request between the regenerative and friction brake systems. However, as this study is focused on decoupled regenerative braking (i.e., actuated independently of the brake pedal), the specifics of the braking controller fall outside the scope of this research.

Lift-off regenerative braking engages when the driver releases the accelerator pedal (i.e., $APP = 0$). The resulting negative torque request is dictated by a control variable, which this study intends to adapt to the driver's preferences. The control variable used in this research is desired deceleration, meaning that the necessary negative torque to achieve that desired deceleration is calculated every time the driver lifts off the accelerator pedal. This calculation is driven by the following vehicle longitudinal dynamics equations:

$$F_T - F_R = m\,\ddot{x}_{des} \tag{14}$$

$$F_T = \frac{\eta_m\,\beta}{R}\,T_m \tag{15}$$

$$F_R = \mu_R\,m\,g + m\,g\sin\gamma + \frac{1}{2}\rho\,C_d\,A_f\,\dot{x}^2 \tag{16}$$

where $\ddot{x}_{des}$ is the desired acceleration, β is the total gear ratio of the drivetrain, R is the loaded radius of the wheels, and μ_R is the estimated rolling resistance coefficient. If we consider vehicle parameters such as mass, gear ratio, and wheel radius to be constant, then the required torque (T_m) to achieve the desired deceleration at any point in time can be calculated dynamically using the signals of vehicle speed ($\dot{x}$), road grade angle (γ) as measured by accelerometer, and motor efficiency η_m as estimated by the manufacturer-provided look-up table. The torque controller follows this process to implement lift-off regenerative braking deceleration:

1. Lift-off regenerative braking activates while $APP = 0$ and $\dot{x} > 0$.
2. Deceleration torque is calculated based on desired deceleration and the measurable signals at the onset of lift-off regenerative braking.
3. Deceleration torque request is saturated to within motor torque limits.
4. The *constant* deceleration torque request is sent to the motor unit while lift-off regenerative braking is active.

3.1.4 Driver Model

A driver model replicating human interactions with the accelerator and brake pedals is crucial for this study. With an accurate model, we can gain insight into how often a typical driver uses the pedals during a drive cycle. In the case of lift-off regenerative braking, the frequency and magnitude at which the driver model must interact with the pedals to match the reference velocity of a simulated drive cycle can be used to reveal any mismatches between the regenerative braking deceleration and the simulated driving pattern.

The driver model implements a longitudinal speed-tracking controller. Based on the vehicle's feedback velocity received from the vehicle body model, the driver model generates normalized acceleration or deceleration commands. These normalized commands are considered as pedal inputs, which are then sent to the torque and braking controllers, respectively. The speed-tracking controller implements an optimal preview method developed by MacAdam to mimic a human driver's ability to look ahead and predict future maneuvers in order to follow a path [83]. The forthcoming discussion provides a brief overview of MacAdam's approach.

The optimal preview control method utilizes linear vehicle dynamics to anticipate a future speed tracking error. The vehicle dynamics implemented by the driver model are outlined below:

$$x_1 = v \tag{17}$$

$$\dot{x}_1 = \frac{K_{pt}}{m} - g \sin\gamma + F_r x_1 \tag{18}$$

where v is longitudinal velocity, K_{pt} is the estimated effective tractive force of the vehicle (a constant), and F_r is the rolling resistance.

The model operates on the premise of using the linear vehicle dynamics to predict an error signal at a specific point in the future based on a preview distance parameter. It then finds the acceleration and deceleration commands (i.e., pedal inputs) that minimizes this previewed error signal. Additionally, it simulates a human driver's response delay by incorporating a driver lag. The chosen values for both the driver lag and the preview distance are meant to reflect the driver's sensory and neuromuscular mechanisms (i.e., driver lag = 0.2 s, preview distance = 2 m).

3.2 Online Driving Condition Identifier Design

In order to adapt the regenerative braking strength to the current environment, an online identification system that is compatible with automotive-grade embedded hardware applications must be developed. This section will discuss the process involved in data gathering, training the clustering model, and implementing the subsequent clusters in a real-time fuzzy inference system for the identification of driving conditions.

3.2.1 Feature Selection

Longitudinal driving conditions are defined by signals like longitudinal displacement, velocity, and acceleration. These signals, obtained from the vehicle's telemetry, can be utilized to extract additional features of the drive cycle, including the number of stops and various statistical parameters such as mean, maximum, and standard deviation of velocity and acceleration. These data points, when systematically collected and analyzed, are then used to find patterns of driving behaviour.

Table 1. Features selected for logging from existing vehicle telemetry.

Feature	**Unit**
Average velocity	km/h
Average positive acceleration	g
Average negative acceleration	g
Standard deviation of velocity	km/h
Standard deviation of positive acceleration	g
Standard deviation of negative acceleration	g
Maximum velocity	km/h
Maximum positive acceleration	g
Maximum negative acceleration	g
Number of stops	count

Table 1 lists the features that are selected to be logged for the purpose of vehicle data clustering. These features have been selected due to being well established in the literature for adequately characterizing driving conditions. This includes the average and maximum values for velocity, positive acceleration, and negative acceleration [18][19], their standard deviation [19][40], and number of stops [40]. In this research, a stop is counted when vehicle speed is less than 8 km/h in order to capture rolling stops. The idea behind selecting a broad range of features is that it results in a greater probability of the characteristic driving conditions being more fully captured and described in the data [84].

3.2.2 Drive Cycle Interval Clustering

To identify clusters of characteristic driving conditions, a dataset of drive cycle intervals and their feature vectors is required. The selected features are collected at specified intervals from a range of simulated drive cycles representing diverse driving conditions. Vehicle telemetry features are logged according to distance traveled in order to prevent distortion caused by idle times and to keep track of the number of stops throughout a drive cycle interval.

Intervals are logged every 500 meters. This enables the collection of a large amount of driving data across multiple drive cycles, thus ensuring that the data is representative of a diverse range of driving conditions. Drive cycle interval data is collected from simulations of 22 transient drive cycles, as listed in Table 2. This data is acquired from simulations of a high-fidelity MATLAB/Simulink vehicle model performing each drive cycle. The final dataset consists of feature vectors representing over 2700 driving intervals collected from the simulated drive cycles.

With the dataset collected, the next step is to discover the underlying clusters of drive cycle intervals that represent different driving conditions. The HDBSCAN algorithm is used in this data exploration task, and the resulting clusters are assessed in order to provide insight into whether the algorithm is suited for identifying meaningful clusters in vehicle data. Ultimately, the success of the data exploration task depends on the ability of the HDBSCAN to accurately group data points into distinct clusters.

When performing a cluster analysis, a critical aspect to address is the identification of the most representative number of clusters within the dataset. While HDBSCAN does not directly require the specification of the cluster count as a predefined hyperparameter, its hyperparameters can be selected and tuned to essentially find any number of clusters. This means that an incorrectly tuned HDBSCAN

model might result in the identification of unsuitable clusters, including excessively large clusters lacking clear distinctions or excessively small clusters with little meaningful relevance. For this reason, having a well-informed estimate of the number of clusters in the dataset is essential to steer the algorithm toward discovering coherent and meaningful clusters, thereby preventing the formation of incoherent or irrelevant groupings. This is especially difficult in datasets where the optimal number of clusters is unknown and must instead be discovered.

Table 2. Selected transient drive cycles for data collection.

No.	Drive Cycle	No.	Drive Cycle
1	Braunschweig City Driving Cycle	12	New York City Cycle (NYCC-LD)
2	California Unified Cycle (UC) LA92 Cycle	13	NREL Class 3 Electric Vehicle Cycle
3	City Suburban Heavy Vehicle Cycle (CSHVC)	14	NREL Utility Truck Cycle
4	Worldwide Harmonized Light Vehicles Test Cycle (WLTC)	15	NREL Parcel Delivery Truck Cycle (Baltimore)
5	EPA Urban Dynamometer Driving Schedule (UDDS)	16	UDDS for Heavy-Duty Vehicles (UDDS-HD)
6	EPA Highway Fuel Economy Test (HWFET)	17	Speed Correction Driving Schedule (SC03)
7	EPA Inspection and Maintenance (IM) 240	18	Fleet DNA Local Delivery Representative
8	EPA US06 Supplemental Federal Test Procedure Driving Schedule	19	Fleet DNA Long-Haul Representative
9	Manhattan Bus Cycle	20	Fleet DNA Regional-Haul Representative
10	New York Bus Composite Cycle (NY Comp)	21	Fleet DNA Transit Bus Representative
11	New York Bus Cycle (NY Bus)	22	Orange County Transit Bus Cycle (US-OCTA)

One such systematic method for determining the optimal number of clusters is the Elbow Method [45]. The Elbow Method is a technique that involves an iterative process of fitting a K-means model for varying values of K and calculating the sum of squared distances at each iteration. The sum of squared distances, also referred to as the "within-cluster sum of squares", is given as:

$$WCSS = \sum_{j=1}^{K} \sum_{i \in C_j} \|x_i - \mu_j\|^2 \quad (19)$$

where K is the number of clusters, x_i is the feature vector at data point i, and μ_j is the feature vector at the centroid of cluster C_j. It quantifies the overall variability or dispersion of data points from their respective cluster centroids, offering insights into the compactness of clusters. A sum of squared distances that is too large suggests that the data points are widely scattered from their cluster centroids, potentially indicating that the clustering is not effectively capturing underlying patterns, whereas a sum of squared distances that is too small may imply overly compact clusters, possibly leading to overfitting and the creation of too many clusters.

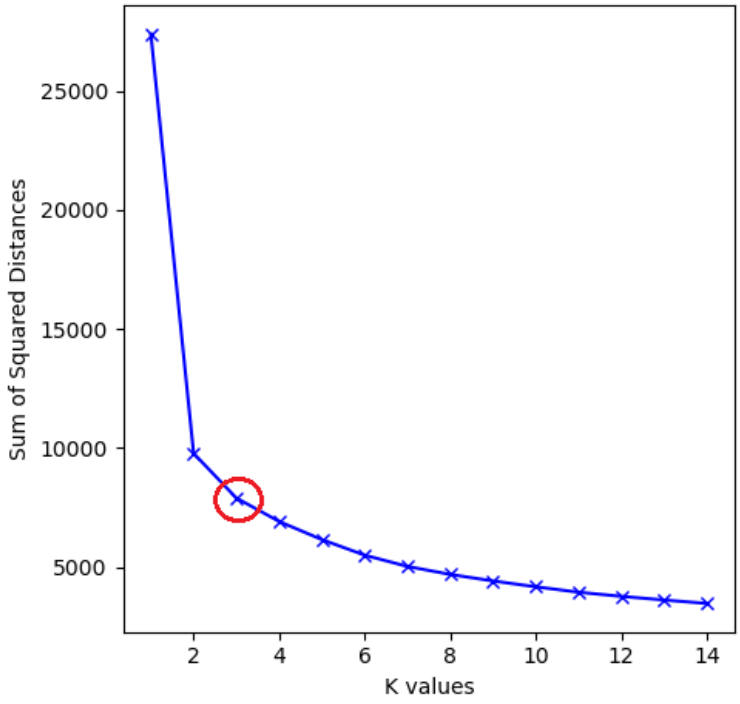

Figure 16. Elbow method plot for drive cycle interval dataset. A K value of 3 (circled) is identified as the elbow point for the sum of squared distances.

As K increases at each iteration of performing the Elbow Method, the sum of squared distances typically decreases, indicating that the data points are closer to their cluster centroids. However, there is a point at which the reduction in this value starts to slow down, resulting in an "elbow" point in the plot. This elbow point represents the optimal number of clusters, as it signifies a balance between

minimizing within-cluster variance and avoiding excessive fragmentation of the data into smaller, less meaningful clusters. From Figure 16, the "elbow" or minimal point at which the slope of the sum of squared distances stabilizes after an observable change in slope can be seen to be at $K = 3$ for the dataset of drive cycle intervals. This indicates that there are likely 3 underlying driving condition clusters within the dataset.

Before training the HDBSCAN model on the drive cycle dataset, the data is first standardized. Data standardization is a preprocessing technique used to transform the values of numerical features in a dataset so that they have a common scale and are centered around a common reference point. Equation 20 shows how this is done by subtracting the mean value of the feature (μ) from each data point (x_i) and then dividing by the standard deviation (σ). The result is that all features have a mean of zero and a standard deviation of one, ensuring that they are comparable and preventing features with larger scales from unduly influencing the results of data analysis or modeling. Standardizing data before fitting a clustering model is crucial because it ensures that all features contribute equally to the clustering process, preventing variables with larger scales from dominating the results.

$$z = \frac{x_i - \mu}{\sigma} \tag{20}$$

After standardizing the data, an HDBSCAN model is tuned to fit to the dataset of drive cycle intervals. A grid search is performed to determine the optimal hyperparameter values for the model, constraining the selection of optimal hyperparameters to those that resulted in an identification of 3 clusters. The hyperparameters that are included in this search are the minimum cluster size, which specifies the minimum number of data points required for a cluster to be formed, and the minimum samples, which determines how many data points must be present within a local neighborhood for it to be considered a core point.

The optimal hyperparameters are determined by selecting the value combinations that resulted in the highest average silhouette score. The silhouette score is a widely employed metric for assessing how effectively data points align with their respective clusters, considering both the average distances within clusters (intra-cluster distance) and the average distances between clusters (inter-cluster distance) [85]. Silhouette score is given by:

$$S(x_i) = \frac{b(x_i) - a(x_i)}{\max\big(a(x_i), b(x_i)\big)} \tag{21}$$

where $b(x_i)$ is the minimum average distance from x_i to data points in a different cluster (inter-cluster distance) and $a(x_i)$ is the average distance from x_i to other data points within the same cluster (intra-cluster distance). The silhouette scores of all data points are averaged in order to evaluate the quality of the model's clusters.

Following a grid search, the optimal hyperparameter values for fitting the HDBSCAN model to the drive cycle interval dataset are found to be a minimum cluster size of 30 and 28 minimum samples. To provide a point of comparison that can be used to assess HDBSCAN's suitability in this data exploration task, a K-means model was also tuned and fitted to the drive cycle interval dataset. The resulting clusters are illustrated in Figure 17.

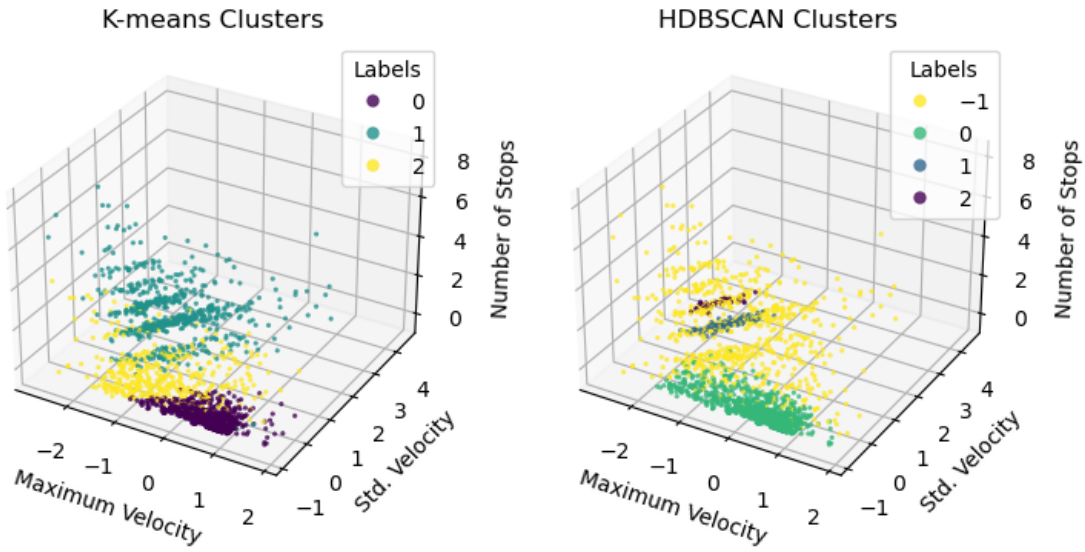

Figure 17. Comparison of clusters identified by HDBSCAN and K-means models fitted to the drive cycle interval data set. A label of -1 indicates discarded noise.

As expected, the K-means model partitions the entire data set into the specified number of clusters. In contrast, HDBSCAN identifies regions of high cluster density and identifies noise with a label of -1. Consequently, the HDBSCAN algorithm is highly selective in defining relevant data points for cluster determination, discarding numerous data points as noise. Upon visually assessing the clusters, it becomes evident that the cluster labeled as 1 in K-means lacks cohesiveness compared to the other clusters. This is illustrated by the distinct linear groupings, or "striations", of data points within the cluster that do not seem to be distributed in relation to a single high-density centroid. In comparison,

the HDBSCAN algorithm identifies distinct striations as their own separate clusters. As a result, the HDBSCAN clusters are visually more cohesive and seem to represent distinct regions of the dataset. This visual assessment aligns with the mean silhouette score of all clustered data points (refer to Table 3), indicating that HDBSCAN clusters yield a score that is 38.9 % higher than that of the K-means clusters.

Table 3. Comparison of silhouette scores for HDBSCAN and K-means clusters.

Model	**HDBSCAN**	**K-means**
Mean Silhouette Score	0.70215	0.50555

By comparing the cluster centroids identified by the HDBSCAN model, the underlying driving conditions that the clustering models seem to have identified can be inferred. Table 4 contains a high-level summary of the feature values at the cluster centroids and the inferred driving conditions for each cluster label. The driving conditions represented by each cluster label are inferred based on existing road classifications (i.e., local road, arterial road, highway) [86]. From the feature values at the cluster centroids, it is clear that there is enough distinction between the clusters to meaningfully differentiate between real-world driving conditions. With that said, the accuracy of the clusters can only truly be evaluated following the simulation and real-world testing of the completed online identification scheme to see if the cluster centroids correspond to coherent driving condition identifications.

Table 4. Inference of driving conditions from HDBSCAN cluster centroids. See Appendix A for all 10 feature values for each cluster centroid.

Label	**Velocity**	**Acceleration**	**Number of Stops**	**Inferred Driving Condition**
0	Highest	Lowest	Lowest	Highway
1	Low	Moderate	Moderate	Arterial
2	Lowest	Highest	Highest	Local

3.2.3 Fuzzy Inference

Fuzzy logic employs approximate reasoning, mimicking human decision-making with vague information. It allows for partial membership between sets of ambiguous boundaries (e.g., “tall”, “beautiful”, “high”). At its core, fuzzy logic introduces the concept of a "fuzzy set," where an element can belong to a set to a certain degree, rather than being strictly in or out of the set. The fuzzy inference system for online driving condition identification is designed such that it has 10 inputs (data features in Table 1), 3 outputs (inferred driving conditions in Table 4), and utilizes "Low," "Medium," and "High" as fuzzy sets to describe all 10 inputs.

In the context of identifying real-time vehicle driving conditions, a fuzzy inference system is particularly advantageous. It enables the incorporation of expert knowledge and linguistic rules, making it suitable for interpreting driving conditions that do not have precise numerical definitions. A fuzzy inference system consists of several components, including a rule base and an inference engine that processes these rules.

Table 5. Correlation of input features to driving conditions using linguistic terms.

Driving condition	**Local**	**Arterial**	**Highway**
Average velocity	Low	Medium	High
Average positive acceleration	High	Medium	Low
Average negative acceleration	High	Medium	Low
Standard deviation of velocity	Medium	High	Low
Standard deviation of positive acceleration	High	Medium	Low
Standard deviation of negative acceleration	High	Medium	Low
Maximum velocity	Low	Medium	High
Maximum positive acceleration	High	Medium	Low
Maximum negative acceleration	High	Medium	Low
Number of stops	High	Medium	Low

The rule base is a database of linguistic rules. It contains a set of "if-then" rules that link the input variables to the output variables. The inference engine then interprets these rules and generates appropriate outputs based on the input data. To construct the rule base, the input features of driving data must be defined by linguistic terms for each possible driving condition. This involves analyzing the feature values located at the centroids of the identified driving condition clusters, and comprehending their relationships with values in other clusters, as outlined in Table 5. The fuzzy rule base, which forms the foundation for inferring driving conditions, is subsequently derived based on these observed correlations in the following manner:

1. If avg. velocity is **low** OR max. velocity is **low**, THEN *driving condition* is **local**.
2. If avg. velocity is **medium** OR max. velocity is **medium**, THEN *driving condition* is **arterial**.
3. If avg. velocity is **high** OR max. velocity is **high**, THEN *driving condition* is **highway**.
4. If avg. positive acceleration is **high** OR std. positive acceleration is **high** OR max. positive acceleration is **high**, THEN *driving condition* is **local**.
5. If avg. positive acceleration is **medium** OR std. positive acceleration is **medium** OR max. positive acceleration is **medium**, THEN *driving condition* is **arterial**.
6. If avg. positive acceleration is **high** OR std. positive acceleration is **high** OR max. positive acceleration is **high**, THEN *driving condition* is **highway**.
7. If avg. negative acceleration is **high** OR std. negative acceleration is **high** OR max. negative acceleration is **high**, THEN *driving condition* is **local**.
8. If avg. negative acceleration is **medium** OR std. negative acceleration is **medium** OR max. negative acceleration is **medium**, THEN *driving condition* is **arterial**.
9. If avg. negative acceleration is **high** OR std. negative acceleration is **high** OR max. negative acceleration is **high**, THEN *driving condition* is **highway**.
10. If std. velocity is **medium** OR number of stops is **high**, THEN *driving condition* is **local**.
11. If std. velocity is **high** OR number of stops is **medium**, THEN *driving condition* is **arterial**.
12. If std. velocity is **low** OR number of stops is **low**, THEN *driving condition* is **highway**.

Membership functions are a key component of a fuzzy inference system, representing the degree to which an element belongs to a fuzzy set. These functions map the input values to a membership degree, providing a basis for decision-making within the fuzzy system. In practice, the design of these functions is guided either by expert knowledge, which offers insights into the data's behavior, or through arbitrary definition, which, in the absence of robust information, can introduce uncertainties and inaccuracies into the system. Ideally, membership functions should be informed by a combination

of domain expertise and empirical evidence to ensure they accurately represent the underlying relationships within the data, leading to more reliable and meaningful inferences.

By designing the membership functions such that they are centered on the feature values of the HDBSCAN cluster centroids, this desired combination of expert knowledge and data-driven empirical evidence is achieved. The resulting membership functions are thus representative of real-world driving conditions as identified by the clustering process, while still preserving important context that can only be provided by foreknowledge (e.g., typical speed limits). For example, the membership functions associated with average velocity illustrated in Figure 18a are centered on their cluster centroid values, while their boundaries are established through informed approximations and iterative fine-tuning. The membership functions for the outputs (i.e., driving conditions) illustrated in Figure 18b are centered around arbitrary values that will later serve as reference points for determining the most probable driving condition.

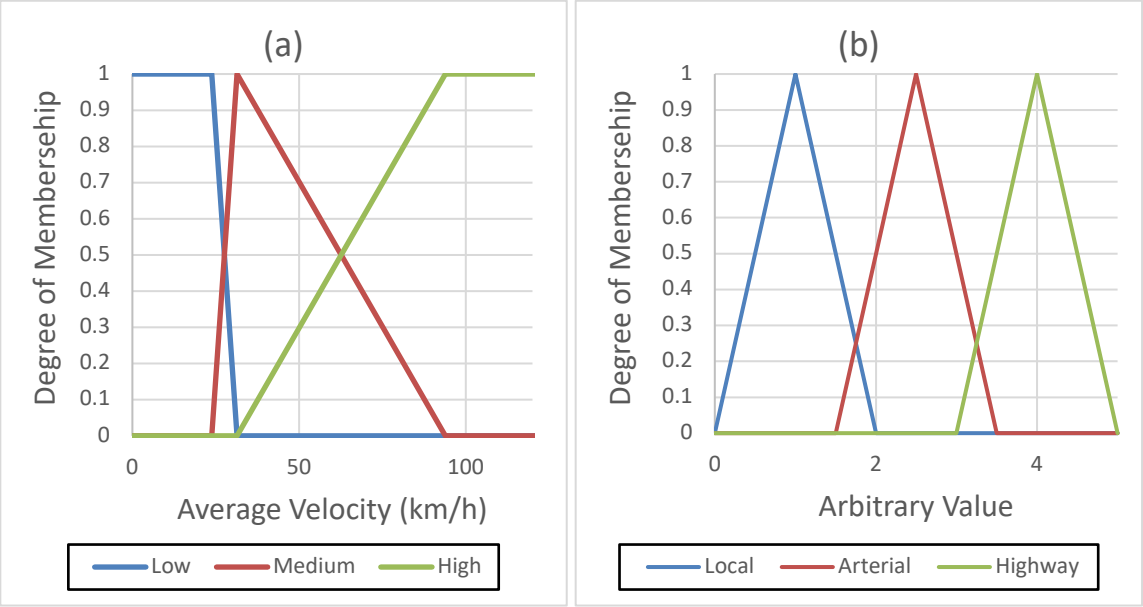

Figure 18. Membership functions for (a) average velocity input and (b) driving condition output.

The proposed fuzzy inference system follows the standard working principles of a Mamdani-type fuzzy logic system. The process used by the online identification scheme for identifying driving conditions in real-time is outlined below:

1. **Fuzzification**: 10 input features from the most recently logged 500-meter interval of vehicle data are converted into fuzzy linguistic variables using membership functions. Each input value is mapped to a numerical value representing its degree of membership in the relevant linguistic term (i.e., "Low," "Medium," "High"). Likewise, the driving condition outputs are mapped to arbitrary values which their membership functions are centered on.
2. **Rule Evaluation**: Each rule from the fuzzy rule base is evaluated by calculating the sum of the degrees of membership of the inputs to the linguistic terms defined in the antecedent of the rule (i.e., the *if* part).
3. **Rule Aggregation**: The degrees of membership to each driving condition from each rule are aggregated using the probabilistic-OR equation:

$$probor(A, B) = A + B - A * B \tag{22}$$

4. **Defuzzification**: The aggregated fuzzy output is converted to a crisp numerical value by finding the maximum of the aggregated probability distribution (i.e., mean of maximum) and taking the associated value of the x-axis.
5. **Labelling**: The distance between the defuzzified value and the arbitrary values that the respective output membership functions are centered on is calculated. The driving condition that is closest to the defuzzified value is selected as the active control label.

3.3 Adaptive Regenerative Braking Controller Design

In this section, the design of an adaptive regenerative braking controller that adjusts to an individual driver's deceleration preferences is discussed. The development of this controller is broken down into steps regarding the establishment of an objective function that accurately represents driver preferences, the formulation of the underlying optimization problem, and the implementation of the Q-learning algorithm to effectively learn the ideal regenerative braking deceleration.

3.3.1 Objective Function

Because human preferences can be complex and challenging to quantify, this research requires the definition of a metric that can effectively represent them. This metric serves as the foundation for the subsequent development of an optimization problem. Previous studies that sought to assess driver acceptability and trust of ADAS features measured driver preferences by analyzing their interactions

with the accelerator and brake pedals when the automated driving systems were in operation [87][88]. Following a similar approach, driver deceleration preferences will be quantified by analyzing pedal interventions during deceleration events.

Within the context of regenerative braking, deceleration events will be considered as moments where the vehicle slows down while the accelerator pedal is not pressed. This means that decelerations that occur while the driver is adjusting the accelerator pedal position or coasting will not be considered since they do not represent decelerations from lift-off regenerative braking. Deceleration events are identified when the following conditions are met:

1. Vehicle velocity is greater than 1 km/h
2. Vehicle acceleration is negative
3. Accelerator pedal position is equal to 0

If all of these conditions are met, data logging is initiated and the accelerator and brake pedal positions are recorded for the duration of the deceleration event. The logging ends when *either* of the following conditions are met:

1. Change in vehicle velocity between 0.5 second time steps is greater or equal to 0 km/h
2. Vehicle velocity is less than 1 km/h

The logged deceleration event is discarded if it is less than 1 second long, since these events are likely in response to sudden braking conditions or otherwise sudden adjustments that are not representative of typical driving. Excluding such brief and anomalous occurrences ensures that the recorded data accurately reflects typical driving behavior and contributes to a more reliable analysis of vehicle performance under everyday conditions. Figure 19 illustrates how deceleration events are identified in real-time using the above conditions.

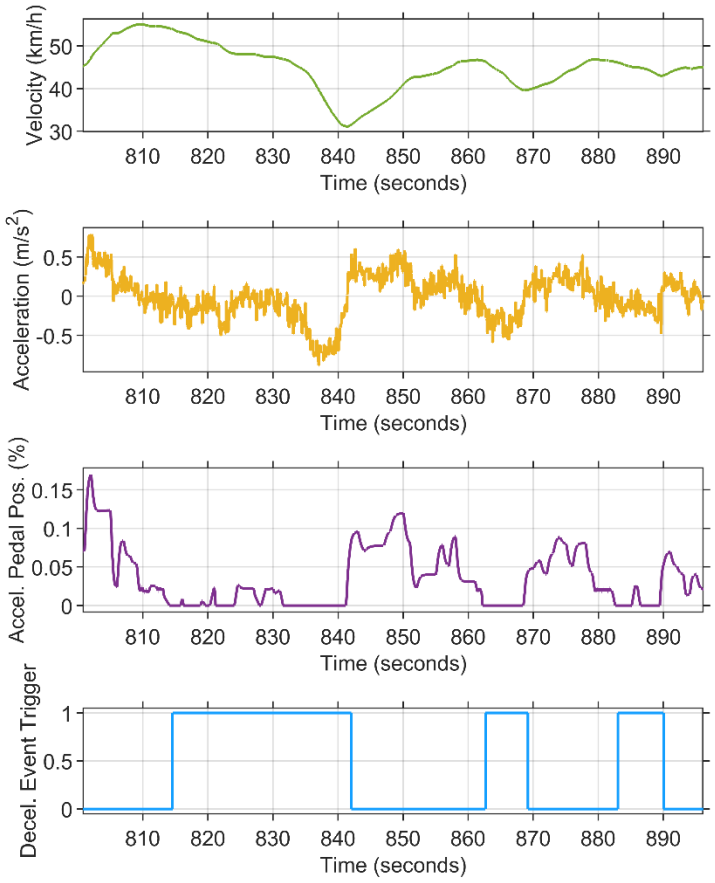

Figure 19. Example of deceleration event detections.

In order to optimize the regenerative braking deceleration to a driver's preferences, an objective function based on pedal interventions must be defined. This research proposes a driver intervention score to serve as a metric for representing how well drivers are satisfied with the rate of deceleration. The driver intervention score is calculated at the end of every deceleration event using logged pedal position data according to Equation 23:

$$Driver\ Intervention\ Score = w_a \frac{a_{lim} - \sqrt{\frac{1}{n_a}\sum_i {a_i}^2}}{a_{lim}} + w_b \frac{b_{lim} - \sqrt{\frac{1}{n_b}\sum_i {b_i}^2}}{b_{lim}} \quad (23)$$

where a and b respectively denote accelerator and brake pedal data, w is a weighting factor to penalize one form of pedal intervention more than the other, a_{lim} and b_{lim} are predefined maximum limits for accelerator and brake interventions, respectively, and n is the number of measurements. The root mean square of the pedal position data is subtracted from and divided by the maximum limit in

order to calculate a relative percentage, with a higher relative percentage denoting less driver interventions. The maximum limits represent the highest root mean square of pedal position data that can be expected across all deceleration events. These limits are determined through empirical observations of simulation data from the drive cycles in Table 2. The parameter values that are selected for the calculation of driver intervention score are listed in Table 6.

Table 6. Selected parameter values for the calculation of driver intervention score.

Parameter	Value
w_a	0.6
w_b	0.4
a_{lim}	0.06 m/s^2
b_{lim}	0.3 m/s^2

Due to the wide range of factors that can cause a decrease in speed (such as slight speed adjustments, coming to a complete stop, or avoiding obstacles), the measurement of the driver intervention score is subject to considerable randomness. This stochastic nature means that the assessment of driver intervention cannot always be precisely attributed to the regenerative braking setting, especially if the driver's actions are influenced by external conditions beyond their control.

To address these fluctuations and ensure a more accurate representation, the driver intervention score is smoothed by calculating the average score based on 5 deceleration events. This process involves discarding the highest and lowest scores and then averaging the remaining 3. By doing so, the variability in the measurement of the driver intervention score is minimized, the impact of unusual occurrences is reduced, and the score becomes a more reliable reflection of the combined effects of the regenerative braking strength and the driving conditions.

3.3.2 Optimization Problem

Finding the ideal regenerative braking strength for an individual driver hinges on the ability to translate the driver's preferences into a tangible optimization challenge. Having defined the proposed average driver intervention score as an objective function to be maximized, the next step is to validate

whether driver interventions do in fact have any bearing on an underlying deceleration preference. This is done by examining the patterns of driver interventions under different driving conditions and varying deceleration intensities, seeing whether the driver intervention score reaches a maximum at the anticipated regenerative braking strength.

For a given deceleration event, let us assume that there is an ideal deceleration rate that precisely corresponds to the driver's preferred trajectory for that particular situation. If the deceleration due to regenerative braking is equal to that ideal rate, then it follows that the driver will not have to intervene with the pedals at all. This means that the regenerative braking strength can be optimized to a driver's preference by tuning the regenerative braking deceleration such that driver intervention score is maximized.

In order to test this hypothesis through simulation, we execute a drive cycle that involves predefined deceleration events with known rates of deceleration. Recall that the driver model used in simulation attempts to match the reference speed of a drive cycle as closely as possible by actuating the pedals. This means that we would expect to see pedal interventions at a minimum when we set the regenerative braking deceleration to the known rate. This further suggests that an ideally matched regenerative braking strength should yield the smallest error between the reference speed specified by the drive cycle and the actual speed of the vehicle since the driver will need to make fewer adjustments to the vehicle's speed during deceleration.

A drive cycle solely comprising of decelerations at a rate of 0.6 m/s^2 is designed. Using the MATLAB/Simulink model environment, multiple simulations are conducted where the lift-off regenerative braking deceleration is iteratively increased in increments of 0.02 m/s^2, ranging from 0.26 m/s^2 to 2 m/s^2 for each iteration of the drive cycle simulation. At the conclusion of each iteration, the average driver intervention score and the average speed error throughout the drive cycle are recorded.

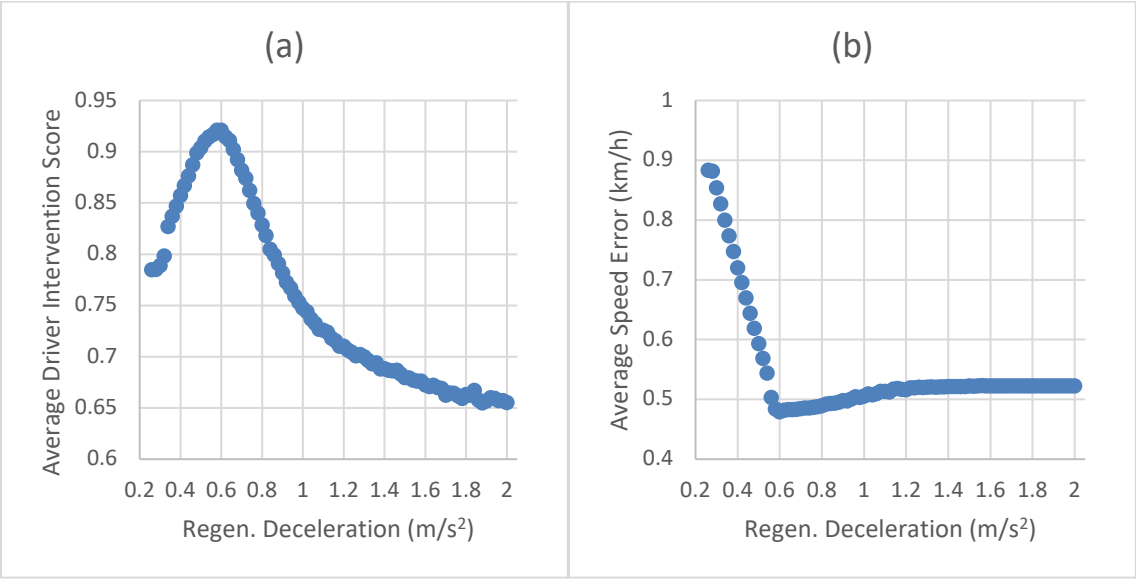

Figure 20. Results from iterating regenerative braking strength in a simulated drive cycle with known decelerations of 0.6 m/s^2 showing the relation between (a) average driver intervention score and (b) average speed error.

The results illustrated in Figure 20 indicate that the hypothesis holds true: aligning the lift-off regenerative braking strength with the desired deceleration rate of 0.6 m/s^2 leads to a peak in the driver intervention score and a minimum in the speed error. The alignment of the peaks and valleys of the evaluation metrics suggests that the proposed driver intervention score truly reflects how closely the vehicle's response corresponds to the driver's intention. Consequently, this score can serve as a reliable indicator of the driver's preferences, even in real-world situations where a reference velocity may not be available. The findings of these simulations also reaffirms the notion that optimizing regenerative braking strength can effectively lessen driver fatigue, assuming the driver's preference for deceleration remains consistent across various deceleration instances under similar driving conditions.

The subsequent phase in ensuring that the driver intervention score is suitable for optimization involves examining whether it is impacted by driving conditions. Drawing from the existing research, we would expect that different driving conditions would have independent objective functions relating regenerative braking deceleration to driver intervention score. To verify this, we apply the same method of incrementing regenerative braking strength across iterations of drive cycle simulations to both the WLTC and UDDS drive cycles. These specific drive cycles are chosen as they

encompass all three driving condition labels according to the online identification system. To ensure that there are enough deceleration events for each driving condition (bearing in mind that the score is computed as the pruned average of 5 events), each drive cycle is repeated 5 times for every iteration.

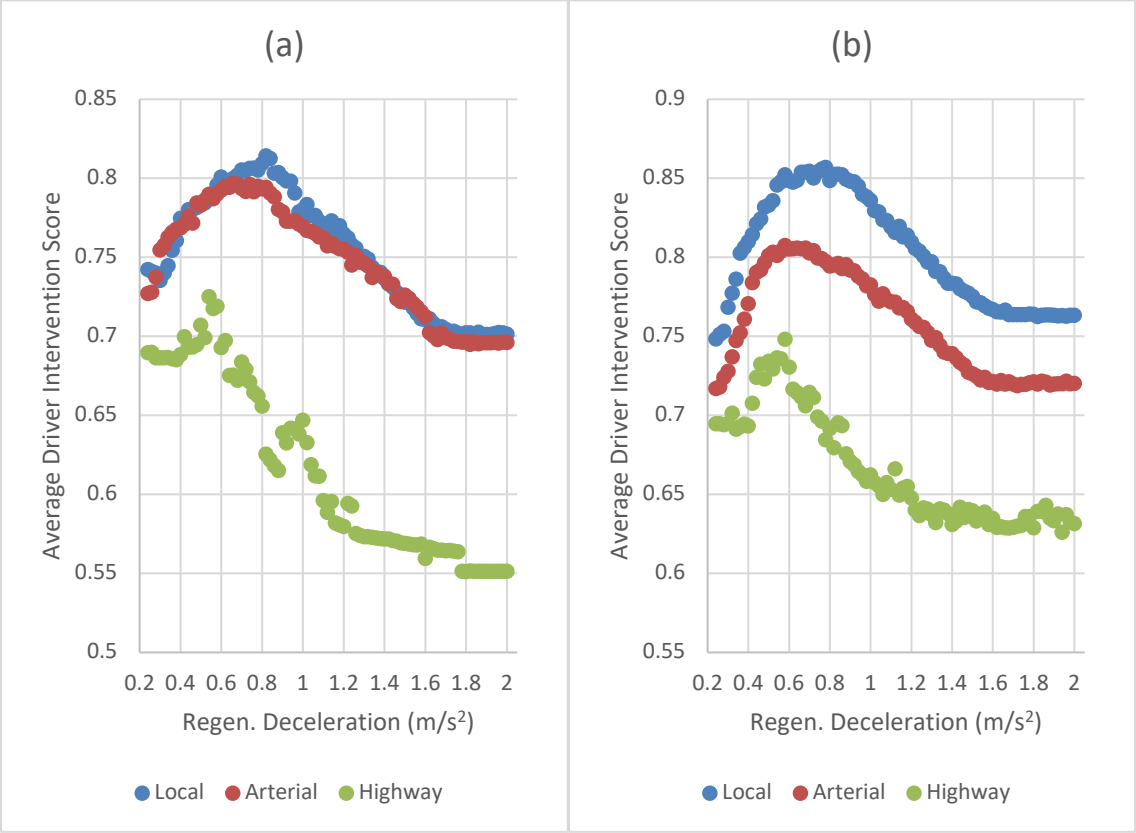

Figure 21. Driver intervention objective functions across driving conditions in (a) UDDS and (b) WLTC drive cycles.

As shown in Figure 21, it is evident that distinct driving conditions are linked with distinct objective functions, each corresponding to a unique optimal regenerative braking strength. For the UDDS drive cycle, the highest driver intervention scores were observed at 0.82 m/s², 0.66 m/s², and 0.54 m/s² for local, arterial, and highway driving conditions, respectively. On the other hand, for the WLTC drive cycle, the peak scores were recorded at 0.78 m/s², 0.58 m/s², and 0.58 m/s² for local, arterial, and highway driving conditions, respectively. This is in line with the expectation that deceleration rates are higher in urban environments and that stronger regenerative braking should lead to fewer driver interventions in local conditions, but more interventions in highway conditions.

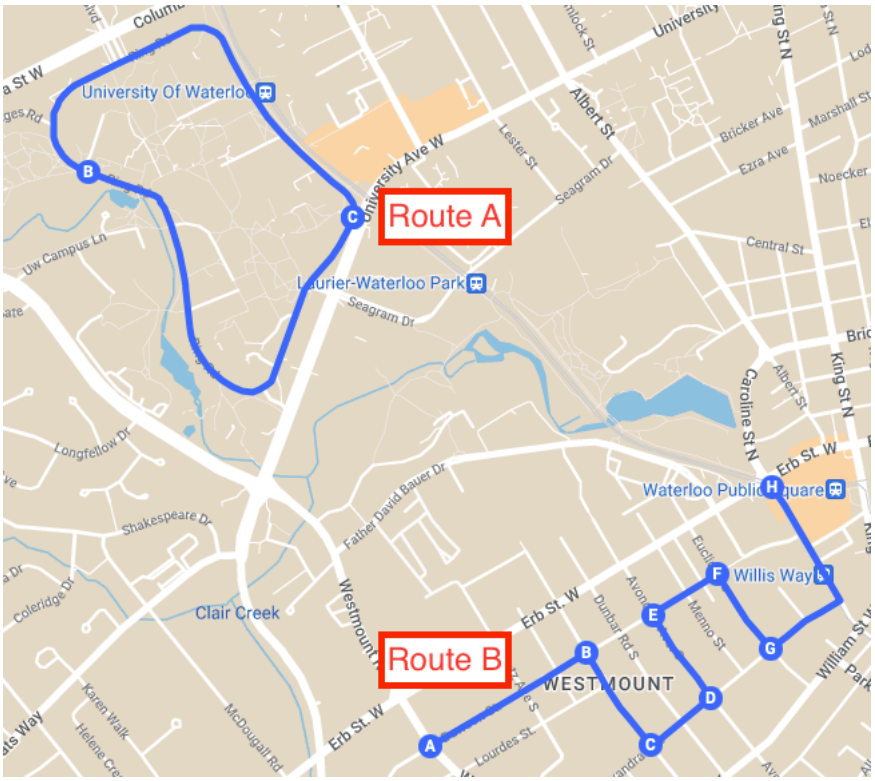

Figure 22. Real-world local drive cycle routes.

So far we have confirmed that the driver intervention score reaches its highest point at a specific desired deceleration rate and varies depending on the driving conditions. To ensure that this score is an appropriate objective function, the final step is to investigate whether the same driver, when driving on different routes of the same driving condition, exhibits similar deceleration preferences throughout. If not, then a learning algorithm would never converge to an optimal regenerative braking strength since the desired decelerations would change with every new route. In accordance with this final validation step, two real-world local drive cycles on separate routes within the vicinity of the University of Waterloo campus (see Figure 22) are recorded with the same driver. The resulting speed profiles for the two drive cycles are illustrated in Figure 23.

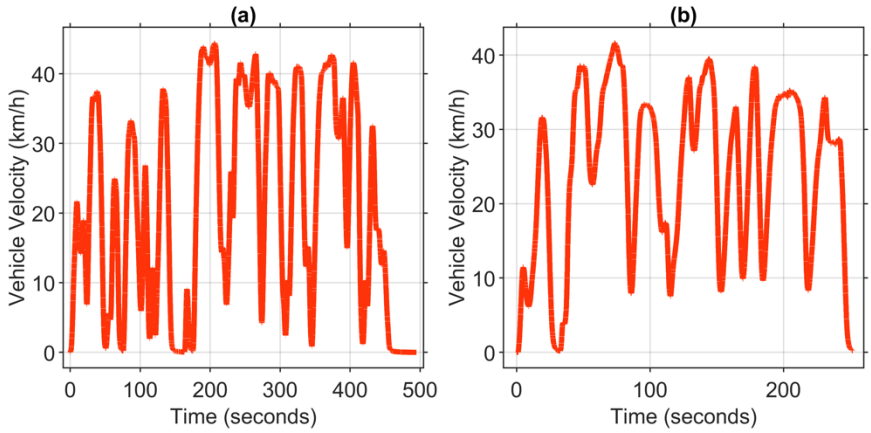

Figure 23. Real-world local drive cycles collected on (a) Route A and (b) Route B.

Following the same approach as before, the two real-world drive cycles are then simulated in the MATLAB/Simulink environment. As demonstrated in Figure 24, the driver intervention score reaches its highest point at 0.76 m/s^2 on Route A and 1.18 m/s^2 on Route B. Despite this disparity, it is important to note that the objective function for Route B is non-convex and has a local maximum at 0.70 m/s^2, which is only 8 % less than the global maximum of Route A's objective function. The minor variation between the peaks indicates that although the absolute best deceleration rates may differ for individual drive cycles on different routes within the same condition, there exists a common local maximum representing the driver's general preferred deceleration rate for that condition.

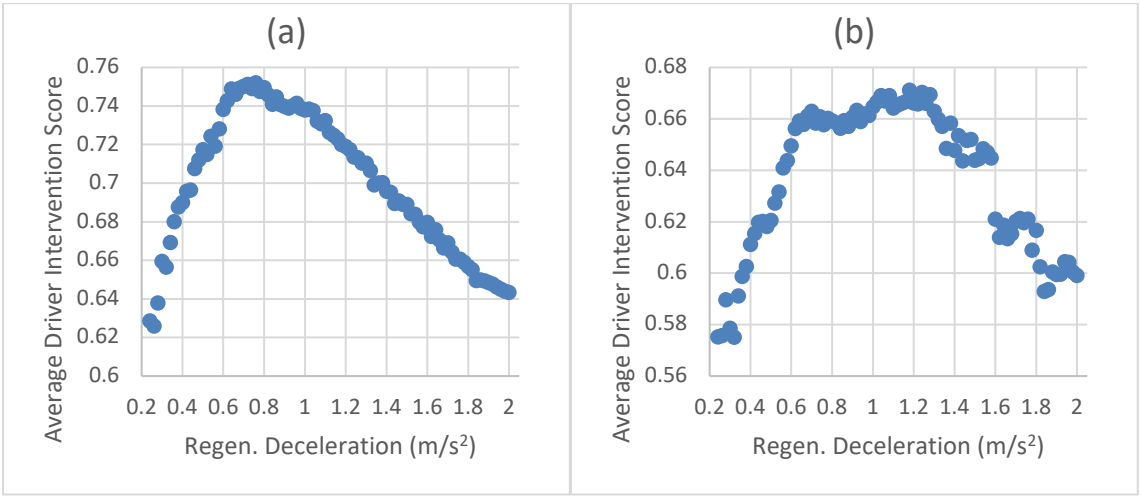

Figure 24. Driver intervention objective functions for real-world drive cycles on (a) local route A and (b) local route B.

Based on these findings, we can infer that the driver intervention score serves as an appropriate objective function for optimizing the regenerative braking deceleration rate. Peak scores coincide with anticipated regenerative braking decelerations when decelerations are known, diverse driving conditions exhibit distinct objective functions, and the same driver shows reasonably consistent deceleration preferences across different routes within the same condition. These attributes suggest that a learning algorithm, capable of navigating non-convex objective functions, can converge to the driver's general preferred deceleration rate for each specific driving condition.

3.3.3 Q-Learning

Having established that each driving condition requires a distinct objective function for optimizing condition-specific regenerative braking strength, the subsequent task is to create an online optimization scheme capable of identifying the optimal regenerative braking strength for each driving condition in real-time. Real-world driving is stochastic and dynamic, making outcomes of deceleration events unpredictable. As shown in Figure 25, the driver intervention score fluctuates significantly across deceleration events despite having the same lift-off regenerative braking deceleration, highlighting the challenge of traversing the objective function using a search algorithm. The algorithm for optimizing regenerative braking strength must therefore be able to handle noisy data and adapt to uncertain environments.

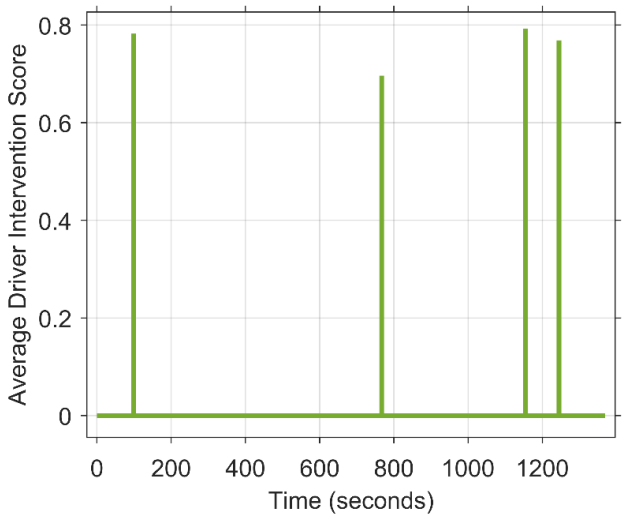

Figure 25. Example of average driver intervention scores triggered after every 5 deceleration events.

Reinforcement learning is well-suited for this online optimization tasks due to its ability to handle environments with unknown dynamics. Reinforcement learning algorithms — also referred to as "agents" — continuously learn from their environments in an iterative fashion. They learn to make optimal decisions through trial and error, updating their knowledge base established on accumulated feedback received from the environment. This makes these algorithms adaptable to changing conditions and capable of finding the best actions to take in real-time, which is essential for online optimization where the environment is dynamic. In this thesis' optimization problem, a reinforcement learning algorithm must update its regenerative braking deceleration selection based on driver intervention score feedback received every 5 deceleration events.

One of the fundamental elements of reinforcement learning is the formulation of the problem as a Markov decision process (MDP). MDP is a control process for making decisions in situations where outcomes are uncertain, and its framework consists of a set of states, actions, and rewards. The process gets its name from the Markov property, which asserts that future states depend solely on the current state and the action taken. Consider a chess game, where the current state represents the positions of all pieces on the board, and the action taken is the move made by one of the players. In this context, the Markov property assumes that the future state of the game (the new board configuration) depends only on the current state (the current board) and the action (the player's move), *without needing to consider all previous moves or game history*.

In order to enable the use of reinforcement learning in the regenerative braking optimization task, an MDP representing the problem at hand must be formulated. The MDP representing the regenerative braking optimization problem is formulated as follows:

1. **States:** The possible set of states S includes all regenerative braking deceleration targets between 0.2 m/s^2 and 2 m/s^2 in increments of 0.08 m/s^2:

$$S = \{x | x = 0.2 + 0.08n, n \in \mathbb{Z}, 0.2 \leq x \leq 2\} \tag{24}$$

2. **Actions:** The possible set of actions A includes taking a negative step in deceleration, staying at the current deceleration, and taking a positive step in deceleration:

$$A = \{-step, 0, +step\} \tag{25}$$

3. **Rewards:** The reward function is based on the relative difference between the current driver intervention score and the best recorded score, followed by a series of conditional rules outlined in Figure 26.

```
# Baseline reward comparing average driver intervention score of current step to best recorded score
reward = 1 - best_score/interventionScore
# Rewards due to relative improvement from previous step
if interventionScore > prevScore:
    reward = reward + 0.1
else:
    reward = reward - 0.1
# Rewards encouraging staying or moving towards the state where the best score was recorded
if current_state == best_state:
    reward = reward + 0.1
else if abs(best_state - current_state) < abs(best_state - prev_state):
    reward = reward + 0.1
else:
    reward = reward - 0.1
```

Figure 26. Pseudo-code representing the reward function of the formulated MDP.

The Q-learning algorithm [89] is of particular interest for the regenerative braking optimization task. Unlike other reinforcement learning algorithms, Q-learning does not require a model of the underlying dynamics of the system, which is especially critical in this application since each driver will interact with the vehicle's regenerative braking system differently. Additionally, Q-learning does not require extensive memory resources, making it a practical and efficient choice for embedded automotive applications.

The Q-learning algorithm operates through an iterative process, aiming to learn the optimal action-selection policy for a given MDP. It accomplishes this by continuously updating a look-up table (known as the Q-table) which contains the expected cumulative rewards (known as Q-values) associated with taking various actions at each state within the MDP. During the execution of the algorithm, an agent interacts with the environment, receiving state information and selecting actions to maximize its long-term reward. A flow chart of this process as it relates to the optimization of regenerative braking is illustrated in Figure 27.

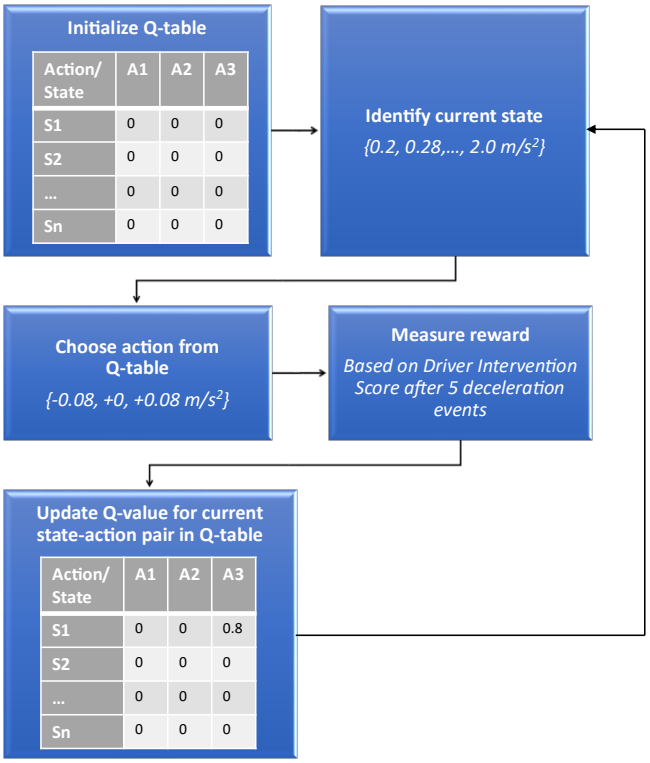

Figure 27. Flowchart of Q-learning process.

The Q-learning algorithm uses a temporal difference approach to update the Q-values in the table based on the received rewards and the Q-values of the next state. This update is driven by the Bellman equation:

$$Q(s,a) = Q(s,a) + \alpha\, R(s,a) + \gamma \max Q'(s',a) \tag{8}$$

where $Q(s,a)$ is the current Q-value for that state-action pair, α is the learning rate, $R(s,a)$ is the reward received for the current state-action pair, γ is the discount rate, and $\max Q'(s',a)$ is the maximum expected future reward for the next state as a result of the current action. The Bellman equation enables the algorithm to refine the estimates of the expected rewards for each action in each state. Through repeated interactions with the MDP, the Q-learning algorithm gradually hones the values in the Q-table, ultimately converging towards the optimal action-selection policy that maximizes the cumulative reward over time.

As the agent continues to explore the MDP, it balances the exploration of new states and actions with the exploitation of the knowledge accumulated in the Q-table, enabling it to make informed

decisions while gradually improving its policy for maximizing long-term rewards. The Q-learning algorithm used in this research is designed such that exploration is high in the early stages of learning, meaning that the agent is more prone to selecting random actions. As learning progresses, the rate of exploration decays exponentially, causing the agent to be more prone to selecting the action with the highest Q-value. Likewise, the learning rate is also designed to decay exponentially, meaning that the Q-values will change less drastically as learning progresses. The full code showing the implementation of the Q-learning algorithm and its exponentially decaying learning parameters is included in Appendix B.

Having designed a Q-learning algorithm to learn the optimal regenerative braking deceleration for an individual driver, the subsequent step involves evaluating its capability to navigate driver intervention objective functions and locate the peaks. The driver intervention objective functions for each driving condition obtained from the simulations of UDDS are used for this evaluation.

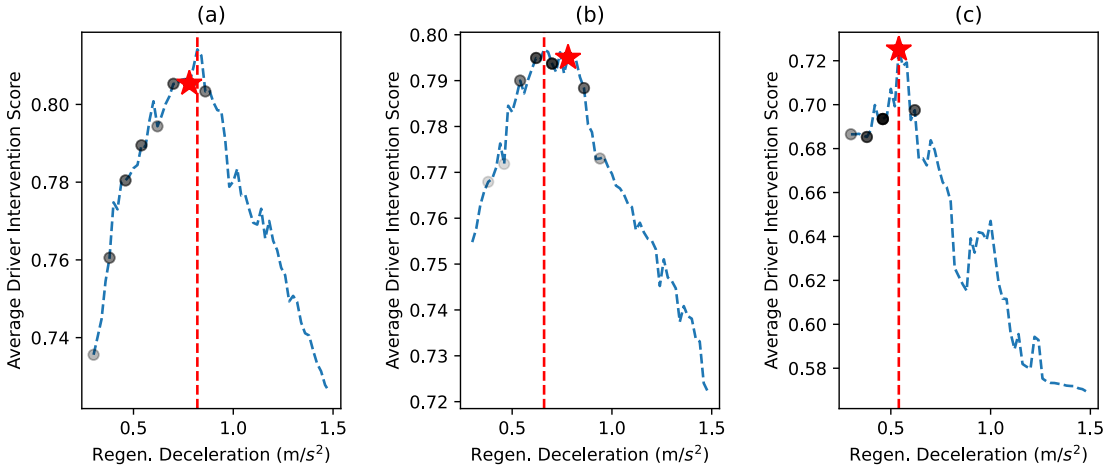

Figure 28. Search paths of Q-learning agent on objective functions of (a) local, (b) arterial, and (c) highway driving conditions in UDDS. The dotted red line indicates the location of the true optimum, the opacity of the black circles represents how often a state is visited, and the red star indicates the final optimal state selected by the agent.

Figure 28 illustrates the algorithm's search trajectory over 100 iterations as the agent hones in on the perceived optimal state for each individual objective function. The agent is able to find the exact peak of the highway objective function, while its optimal states for the local and arterial objective functions are associated with an error of 4.9 % and 18.2 %, respectively. The large error associated

with the arterial driving condition is mostly due to the fact that the objective function contains a plateau rather than a distinct peak. As a result, this error can be deemed insignificant when we consider that the difference in driver intervention score between the true peak at 0.66 m/s^2 and the selected optimum of 0.78 m/s^2 is only 0.2 %. Another source of error is that the step size of 0.08 m/s^2 often does not allow the agent to land on the precise peak of the objective function. However, through experimentation with smaller step sizes, it was discovered that the agent's likelihood of getting trapped in local optima increased. Opting for a larger step size enables the agent to navigate through noisy, non-convex data, which is necessary for the real-world implementation of the algorithm. Keeping the step size at 0.08 m/s^2 allows the agent to follow the overall trend path rather than getting stuck on individual fluctuations in the objective function, while also leading to acceptable accuracy.

3.3.4 Control Process

The following is a summary of the overall control process for the adaptive regenerative braking controller:

1. Three Q-learning agents for each respective driving condition are initialized. The initial regenerative braking deceleration rate for all driving conditions is selected as 0.5 m/s^2.
2. During vehicle operation, the controller receives a driving condition label from the online driving condition identifier at every 500-meter interval.
3. The Q-learning agent for the active driving condition label receives a reward based on the driver intervention score for the past 5 deceleration events.
4. The Q-learning agent selects an action to decrease, maintain, or increase the desired regenerative braking deceleration for the current driving condition.
5. The desired regenerative braking deceleration is output to the vehicle’s torque controller.
6. Steps 2-5 are repeated indefinitely, with the controller’s exploration and learning rates decaying exponentially at every 25 deceleration events.

3.4 Simulation Methodology

In this section, the methodology for evaluating the performance of the adaptive regenerative braking controller will be discussed. The online driving condition identifier is tested in isolation before the combined adaptive regenerative braking control system is tested as a whole.

3.4.1 Online Driving Condition Identifier

The online driving condition identifier is implemented in the MATLAB/Simulink environment containing the target electrified vehicle model discussed in Section 3.1. The driving condition identifications based on HDBSCAN-informed fuzzy inference are compared with a simpler baseline scheme across drive cycle simulations. This baseline scheme uses only average velocity measurements and compares them with the corresponding HDBSCAN cluster centroids via Euclidian distance in order to make its online identifications.

The drive cycles selected for simulation testing represent a comprehensive variety of driving conditions. Firstly, the ARTEMIS Urban, Road, and Motorway cycles [90] are selected since the drive cycles individually specify different driving conditions, so the expected "ground truth" of driving conditions is generally known from the names of the drive cycles themselves. These drive cycles contain different driving conditions that are experienced throughout three known driving scenarios, as specified in the drive cycle names. In fact, the ARTEMIS drive cycles are designed based on a total of 12 driving conditions derived from speed profiles, confirming that these drive cycles do in fact demonstrate transient driving conditions. Secondly, the WLTC drive cycle is selected since it clearly delineates between phases of different driving conditions throughout the cycle, making the determination of the ground truth straightforward.

The identification schemes are evaluated based on their accuracy when compared to the ground truth driving conditions as well as their stability. The accuracy of each scheme's predictions across the drive cycle segments is calculated based on distance traveled with the correct identification label. The stability of the predictions is determined based on how many transitions of the identification labels occur throughout the drive cycle.

3.4.2 Adaptive Regenerative Braking Controller

The combined online driving condition identification and adaptive regenerative braking control scheme is implemented into the torque controller of the vehicle model in the MATLAB/Simulink environment. Through this setup, simulations of UDDS and WLTC drive cycles are executed. These particular drive cycles are deliberately selected as they encompass all three driving conditions, facilitating a comprehensive evaluation of the proposed control scheme's effectiveness across diverse driving scenarios.

Throughout these simulated drive cycles, we record the regenerative braking deceleration rate determined by the Q-learning agent alongside the average driver intervention score for each respective driving condition. The performance of the adaptive regenerative braking controller is evaluated through both qualitative and quantitative analyses. Qualitatively, we examine the convergence of the deceleration rate, while quantitatively, we assess the change in the average driver intervention score throughout the drive cycle. Notably, a reduction in interventions implies enhanced driving comfort, making it a crucial indicator of the controller's effectiveness.

3.5 Real-World Experiment Methodology

As with the simulation methodology, the two components of the adaptive regenerative braking controller are tested individually through real-world experimentation. For experiments of both systems, the same controller used in simulation testing is refactored for real-time hardware. It is flashed onto a dSPACE MicroAutoBox II, which is an automotive-grade controller used in vehicle prototyping. The embedded hardware compatibility of the online driving condition identifier and the combined adaptive regenerative braking controller are assessed by the successful flashing and uninterrupted real-time performance of both systems. The controller is deployed on a FHEV designed by the University of Waterloo Alternative Fuels Team (UWAFT) as part of the EcoCAR Mobility Challenge.

Figure 29. Electrified test vehicle designed by UWAFT used for real-world experiments.

3.5.1 Online Driving Condition Identifier

The test vehicle is driven on a real-world drive cycle of known driving conditions based on road classifications as specified in the Ontario Road Network [91]. The route of this real-world drive cycle is designed to represent known transitions between “local road” and “arterial road” conditions. The drive cycle route is planned in the vicinity of the University of Waterloo campus. As illustrated in Figure 30, it begins with a driving segment on local roads, followed by a segment on arterial roads, and finally concluded with a return to local roads for the last segment of the drive cycle. This is meant to test the online identification scheme’s performance across real-world transitions in driving conditions. Note that the local driving segments occur on Route A (Figure 22).

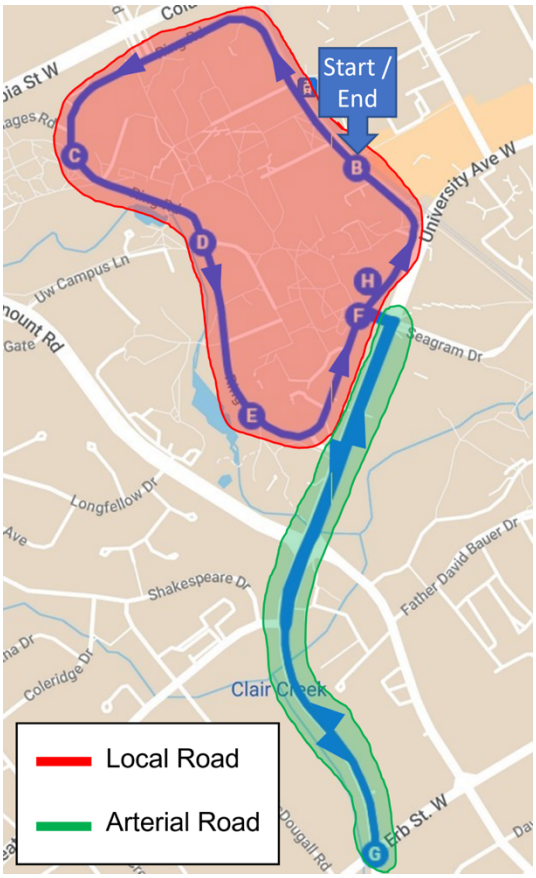

Figure 30. Driving route for online driving condition identifier experiment.

Driving condition labels are collected from the embedded vehicle controller throughout the drive cycle. As with the simulations, the labels produced by the fuzzy inference system are evaluated against a baseline identification scheme driven by average velocity only. This evaluation is done by

comparing their accuracy (based on distance traveled with the correct label) and stability (based on the number of label transitions).

3.5.2 Adaptive Regenerative Braking Controller

The adaptive regenerative braking control scheme is tested by continuously driving the test vehicle with the same driver, while the Q-learning agent learns the driver's preferred rate of deceleration during lift-off regenerative braking. To manage the duration of the experiment, the vehicle is exclusively driven on a local road segment. This approach avoids impractical experiment durations that would arise if numerous deceleration events across all three driving conditions were necessary for the agent to converge to the desired deceleration rates for each driving condition. Furthermore, the reduced speeds in local driving conditions help mitigate the associated risks when testing an experimental controller in real-world environments. The local road segment used in this experimentation is Route A from the online driving condition identifier test.

While the adaptive regenerative braking controller is engaged, the average driver intervention scores are documented over the entire drive cycle. The drive cycle is then repeated twice. Firstly, a constant regenerative braking deceleration of 0.5 m/s^2 is used as a conservative baseline, and secondly, a constant regenerative braking deceleration of 1.6 m/s^2 is employed as an aggressive baseline. The value of the conservative baseline is arbitrarily made equal to the starting point from which the Q-learning agent begins its search of the optimal deceleration rate, thereby representing what the deceleration would be if the same scheme were used with no Q-learning agent. Conversely, the aggressive baseline value is derived from the publicly available deceleration rate for lift-off regenerative braking in the BMW i3 [92], serving as a representative example of the deceleration rates commonly employed by manufacturers [78].

In a similar approach to the simulation testing, the regenerative braking deceleration rate and the average driver intervention score throughout the continuous repetitions of the local road segment are analyzed. The performance of the adaptive controller is assessed by examining the convergence of the Q-learning agent as well as the change in the average driver intervention score throughout the drive cycle. The average driver intervention scores are compared against those collected from the baseline deceleration rates.

Chapter 4
Results and Discussion

The present section provides an analysis of the results obtained from the evaluation of the online driving condition identifier and the adaptive regenerative braking control scheme, which are discussed in separate sub-sections. Initially, a comparison is drawn between the driving condition identifications based on the HDBSCAN-informed fuzzy inference and a simpler baseline scheme utilizing average velocity measurements. Subsequently, the evaluation extends to the implementation of the adaptive regenerative braking control scheme, which is compared with a baseline implementation that is representative of an industry-standard. The results span two testing phases for each sub-section: a simulation phase performed within the MATLAB/Simulink environment on various simulated drive cycles, and a real-world experimentation phase where the embedded hardware compatibility and real-time performance of the control scheme is assessed.

4.1 Online Driving Condition Identifier

The online driving condition identifier was evaluated across simulation and experimental tests. Across these tests, two variants of the online identification scheme were compared in order to highlight the advantages of the proposed identifier over a simpler method. These variants consisted of the HDBSCAN-informed fuzzy inference system (FIS) and the baseline system (B) driven by average velocity measurements only.

4.1.1 Simulation Results

The two variants of the online identification scheme were implemented into the same MATLAB/Simulink vehicle model used to collect the clustering data. The efficacy of the driving condition identifications, comparing HDBSCAN-informed fuzzy inference with a simplified baseline scheme, was examined across various drive cycle simulations across two test cases. For the first simulation test case, the performance of the online driving condition identifier was assessed on three drive cycles each representing a different driving condition. These drive cycles are the ARTEMIS Urban, Road, and Motorway cycles. For the second simulation test case, the identifier's ability to transition between all driving conditions within a single drive cycle was evaluated. The drive cycle used for this test case was the WLTC.

4.1.1.1 Test Case 1: Drive cycles with single dominant driving condition

All three ARTEMIS drive cycles were simulated, with the expectation being that the majority of identification labels would correspond with the nominal driving condition stated in the drive cycle name (i.e., Urban, Road, Motorway). As such, the main quality being evaluated in this test case is the stability of the predicted driving condition label throughout the drive cycles, with the assumption that good performance is characterized by a greater proportion of the predicted labels associated with the dominant driving condition label as well as fewer label transitions throughout the drive cycle.

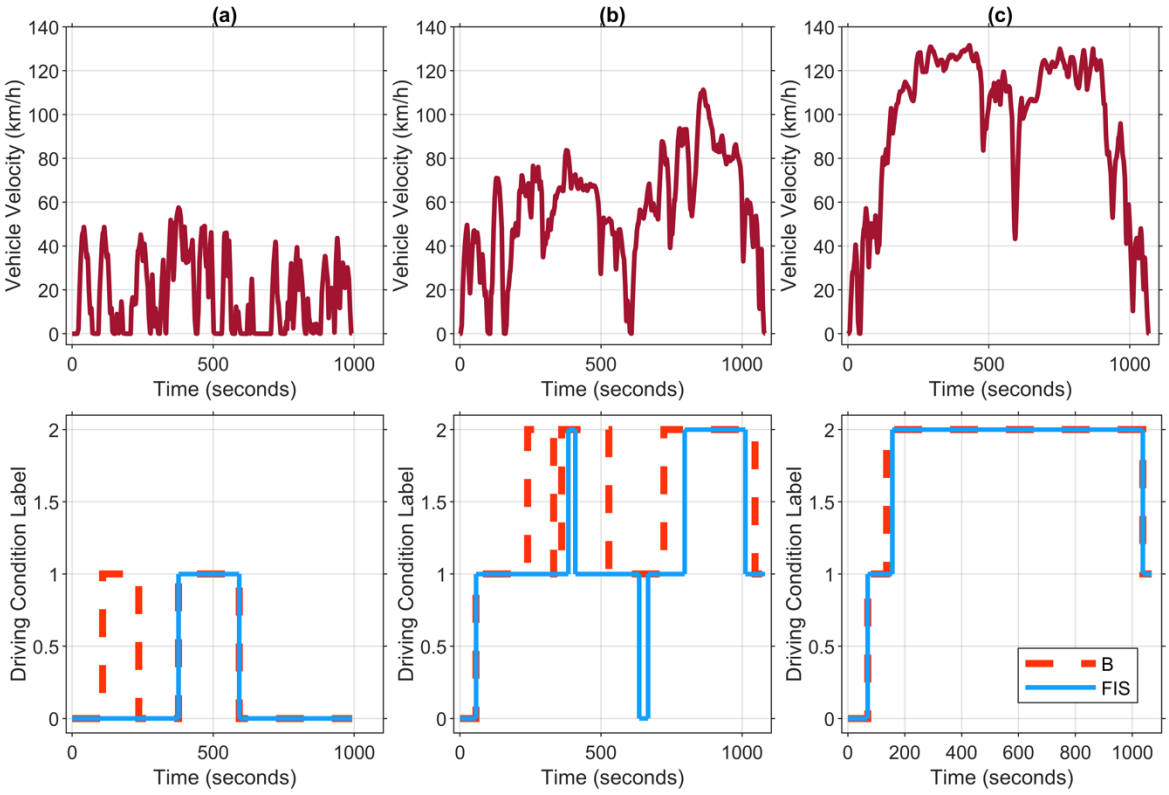

Figure 31. Online driving condition identifications across simulated ARTEMIS (a) Urban, (b) Road, and (c) Motorway drive cycles.

The resulting online identifications are illustrated in Figure 31, where labels of 0, 1, and 2 denote local, arterial, and highway driving conditions, respectively. The identifications produced by the FIS demonstrated notable distinctions from those generated by the baseline variant across all three cycles, emphasizing the substantial impact of additional cluster features beyond average velocity on driving condition predictions. The HDBSCAN-based identifications exhibited reduced sensitivity to velocity

fluctuations, leading to delayed or entirely avoided label transitions. Consequently, a visual inspection of the identification trace over time indicates a more stable driving condition label signal for the FIS compared to the baseline system. This improved stability can be attributed to the augmented "inertia" resulting from the incorporation of all ten cluster features, thereby dampening the system's sensitivity to individual measurements.

The quantitative results of the ARTEMIS drive cycle simulations are summarized in Table 7. When examining the frequency of label transitions throughout each drive cycle, it becomes evident that both the FIS and the baseline scheme generally identified a similar number of transitions. However, in the Urban cycle, the FIS identifies 2 fewer label transitions compared to those detected by the baseline scheme. If we consider each ARTEMIS drive cycle as predominantly indicative of a single driving condition, a decrease in transitions away from this dominant condition can be interpreted as an improvement in performance due to a more consistent driving condition label. This in turn can lead to a more predictable regenerative braking response, thereby contributing to a smoother overall driving experience. In this regard, the FIS outperforms the baseline scheme in local driving conditions.

Table 7. Summary of online driving condition identifications across simulated ARTEMIS drive cycles. The dominant driving condition for each drive cycle is shaded in grey.

ARTEMIS Drive Cycle	Online ID Variant	Label Transitions	Proportion of Local Labels (%)	Proportion of Arterial Labels (%)	Proportion of Highway Labels (%)
Urban	Baseline	4	60.0	40.0	0.0
	Fuzzy Inference System	2	70.0	30.0	0.0
Road	Baseline	7	2.9	31.4	65.7
	Fuzzy Inference System	7	5.7	62.9	31.4
Motorway	Baseline	3	1.8	5.3	92.9
	Fuzzy Inference System	3	1.8	7.0	91.2

Regarding the amount of time spent with the dominant driving condition label, if we designate the dominant driving conditions for the Urban, Road, and Motorway cycles as local, arterial, and

highway, respectively, then a more precise online identifier would be characterized by a higher proportion of driving condition labels corresponding to the dominant driving condition. Both schemes identified a similar proportion of driving conditions within the Urban and Motorway cycles, with the differences in dominant label proportion being the result of only one 500-meter interval of the drive cycle being labelled differently. However, the FIS performs significantly better than baseline in the identification of arterial driving conditions, identifying the dominant driving condition 62.9 % of the time when compared to the baseline's 31.4 %. This doubling of dominant label identifications can once again be explained by the FIS' reduced sensitivity to any one single cluster feature, leading to enhanced stability at the boundaries between driving conditions. This can be extrapolated to say that the HDBSCAN-informed FIS would produce driving condition labels that would result in more appropriate changes to the regenerative braking strength.

Although the simulations of the ARTEMIS drive cycles offer a broad perspective on the stability of the online driving condition identifier, the proportion of the dominant driving condition label serves only as a general gauge of the identifier's accuracy. These simulations do not provide definitive insights into whether label transitions within each drive cycle were accurate or erroneous, as it remains unclear whether these drive cycles were intentionally designed to incorporate specific sections representing distinct driving conditions. The ARTEMIS drive cycles are each composed of transient driving conditions that are not immediately apparent beyond visual inspection of the drive cycle velocity traces. This is especially the case for drive cycles that transition across a range of velocities, such as ARTEMIS Road. In order to evaluate the accuracy of the predictions, the identifier needs to be tested on a drive cycle whose driving conditions are known *a priori*.

4.1.1.2 Test Case 2: Drive cycle with all three driving conditions

The WLTC drive cycle clearly delineates between phases of different driving conditions, making it possible to evaluate the accuracy of the online driving condition identifier. This was done by comparing the predicted driving condition labels with the ground truth throughout the drive cycle. The WLTC is composed of four speed phases as outlined in Table 8. While these speed phases do not directly line up with the three driving conditions identified through HDBSCAN clustering, we can infer the driving condition that represents each phase the best by comparing the characteristic parameters of each phase to the values of the cluster centroids. The "Low" phase is most similar to

the local driving condition, the “Medium” phase is most similar to the arterial driving condition, and both “High” and “Extra High” phases are most similar to the highway driving condition.

Table 8. Characteristic features of each phase of WLTC [93].

Phase	Duration (s)	Time-stamp (s)	Stop Duration (s)	Max. Velocity (km/h)	Avg. Velocity (km/h)	Min. Accel. (m/s^2)	Max. Accel. (m/s^2)
Low	589	0	156	56.5	25.7	-1.47	1.47
Medium	433	589	48	76.6	44.5	-1.49	1.57
High	455	1022	31	97.4	60.8	-1.49	1.58
Extra High	323	1477	7	131.3	94.0	-1.21	1.03

The online identifications throughout the simulated WLTC drive cycle are illustrated in Figure 32, while the corresponding quantitative results are outlined in Table 9. The FIS exhibited significant improvement compared to the baseline in identifying local and arterial driving conditions, achieving a 16.5 % and 10.2 % increase in accuracy, respectively. The improvement in accuracy for these conditions confirms that incorporating all 10 cluster features into the inputs of the fuzzy inference system enhances the online identifier's ability to accurately differentiate between driving conditions. This conclusion stems logically from the notion that gathering a broader range of vehicle data increases the likelihood of fully capturing the characteristics of distinct driving conditions. Both variants of the online identifier performed identically in highway conditions, suggesting that vehicle velocity was the primary indicator of highway conditions in this particular drive cycle.

Table 9. Summary of online driving condition identifications in simulated WLTC drive cycle.

Online ID Variant	Identification Accuracy (%)			
	Local	Arterial	Highway	Overall
Baseline	50.6	79.7	77.4	69.2
Fuzzy Inference System	67.1	89.9	77.4	78.1

When assessing accuracy across the entire drive cycle, the FIS demonstrated an overall accuracy of 78.1%, surpassing the baseline variant's 69.2 % accuracy. This 8.9 % enhancement suggests that utilizing HDBSCAN clustering in the development of a data-driven fuzzy inference system would yield more dependable predictions of driving conditions, at least in simulation. However, although the correlation of driving conditions with different speed phases of the WLTC cycle facilitated a broad evaluation of the online identifier's accuracy, this mapping remains an estimation rather than an absolute determination of ground truth. For example, even though we associated the "Low" speed phase with local driving conditions, Figure 32 illustrates a brief period between 200 seconds and 350 seconds of the drive cycle characterized by a temporary increase in speeds and reduced stops, potentially justifying its classification as an arterial driving condition. Nonetheless, as the entire phase is designated as indicative of local driving conditions, the assignment of arterial conditions by both versions of the online identifier is deemed to be inaccurate.

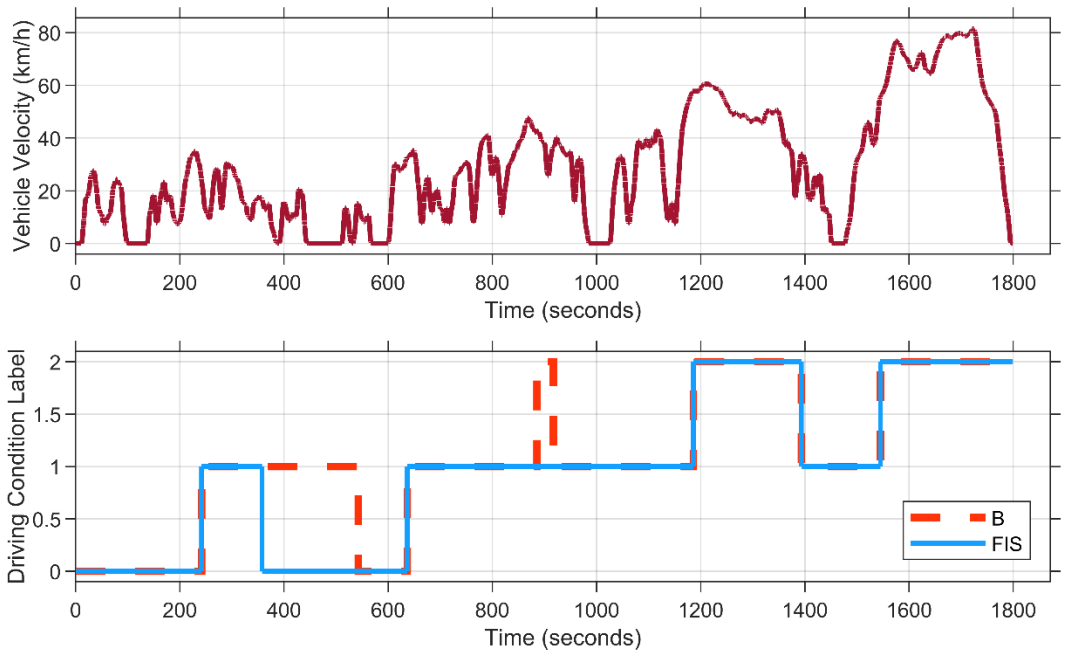

Figure 32. Online driving condition identifications across simulated WLTC drive cycle.

To achieve a more precise assessment of driving condition label accuracy, we must create a customized drive cycle with a more detailed classification of driving conditions. Conducting this customized drive cycle in real-world settings would enable us to explicitly determine the ground truth at every moment for a more precise calculation of accuracy.

4.1.2 Experimental Results

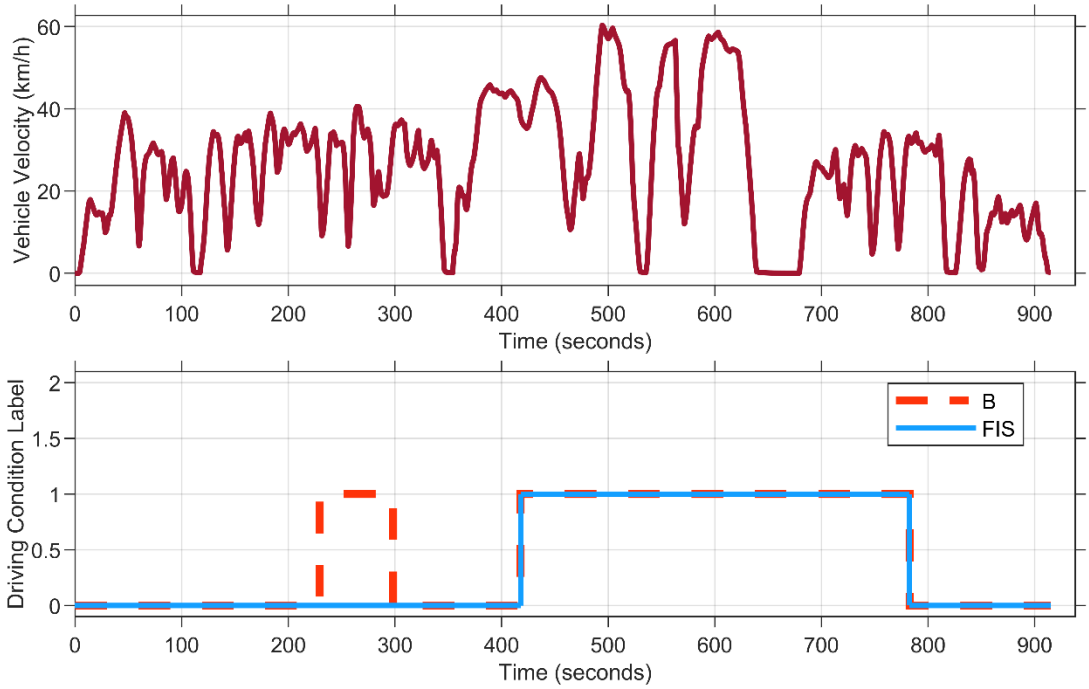

Figure 33. Online driving condition identifications during real-world drive cycle while deployed on embedded hardware.

The online driving condition identifier was successfully flashed onto the MicroAutoBox II embedded controller, thereby confirming its compatibility with real-time hardware applications. A real-world drive cycle representing local and arterial driving conditions was performed using the UWAFT test vehicle. The transitions between driving condition segments were logged, allowing for an establishment of a precise ground truth throughout the drive cycle. The characteristics of each drive cycle segment are listed in Table 10.

Table 10. Characteristics of real-world drive cycle segments.

Characteristic	Local Segment 1	Arterial Segment 1	Local Segment 2
Distance (m)	2387	2966	1237
Duration (s)	352	325	238
Timestamp (s)	0	352	677

The real-time driving condition identifications, recorded by the online identifier while both the FIS and baseline versions were operating concurrently, are depicted in Figure 33. The FIS identifications demonstrated superior stability compared to the baseline, notably excluding an incorrect shift to an arterial driving condition label at roughly 180 seconds, as observed in the baseline identifications. This supports the findings from the simulation testing, in which the FIS identifications also exhibited greater stability. Additionally, both versions of the identifier accurately recognized the actual transitions between local segment 1 and arterial segment 1, as well as between arterial segment 1 and local segment 2. This implies that the HDBSCAN-based online driving condition identifier is capable of effectively detecting driving condition changes, even in the presence of challenges often encountered during real-world testing, such as signal noise and time synchronization issues. This further supports the system's compatibility with real-time applications.

Table 11. Summary of online driving condition identifications in real-world drive cycle.

Online ID Variant	**Identification Accuracy (%)**		
	Local	**Arterial**	**Overall**
Baseline	68.9	79.2	74.1
Fuzzy Inference System	82.6	79.2	80.9

Comparison between logged driving condition labels and real-world ground truth, detailed in Table 11, revealed that FIS identifications improved overall accuracy by 6.8 %. This improvement primarily stemmed from more accurate identifications of local driving conditions, with the FIS correctly identifying local conditions for 82.6 % of segments, compared to the baseline scheme's 68.9 %. The FIS's reduced sensitivity to velocity led to fewer erroneous label transitions, consistent with findings from simulation testing. Both online identifier variants performed identically during the arterial segment, with inaccuracy mainly due to label transition delays from the 500-meter sampling interval.

The accurate identification of driving conditions and the reduction in misidentified transitions imply that using the proposed FIS-based online driving condition identifier with an adaptive regenerative braking controller would facilitate a more effective learning process compared to a simpler identification scheme like the baseline variant in this study. This is because incorrect driving

condition labels would result in the wrong Q-learning agent being activated, thereby causing the agent to learn a regenerative braking strength for the wrong driving condition.

The experimental tests of the online driving condition identifier successfully met the research objectives of compatibility with automotive-standard embedded hardware and accurate driving condition identification through the innovative application of HDBSCAN clustering. To fulfill the remaining goals, the online driving condition identifier will be combined with an adaptive regenerative braking controller to determine a driver's optimal regenerative braking strength according to the driving condition labels.

4.2 Adaptive Regenerative Braking Controller

The adaptive regenerative braking (ARB) controller was constructed by combining the online driving condition identifier with the Q-learning agent. The performance of the ARB controller was assessed through qualitative and quantitative analyses in simulation and real-world testing environments, following a similar methodology to what was done to evaluate the online driving condition identifier. The ARB control scheme was simulated by integrating it within an electrified vehicle torque controller that was first tested in MATLAB/Simulink before being flashed onto the embedded supervisory controller of a real-world electrified vehicle for experimental testing. The ARB controller was evaluated based on its ability to converge to a desired deceleration rate that resulted in fewer driver interventions.

4.2.1 Simulation Results

The ARB control scheme was first tested in a simulation of the UDDS drive cycle. The drive cycle was repeated until all three Q-learning agents associated with each driving condition converged to a deceleration rate. The convergence criterion was defined as the moment at which all three agents went a full two drive cycles without changing the desired lift-off regenerative braking deceleration.

The search path of all three Q-learning agents throughout the repeated UDDS drive cycles is illustrated in Figure 34. The convergence criterion was met after 14 repetitions of the drive cycle, which corresponds to approximately 169 kilometers of driving. The convergence of the ARB scheme was mainly encumbered by the low frequency of deceleration events in highway driving conditions, thereby slowing down the learning process for that agent. The agent associated with local driving conditions was the first to initially stabilize its deceleration output, doing so within 36 kilometers of

driving. However, a subsequent exploration phase interrupted its convergence. The agent that converged the soonest was the one associated with arterial driving conditions, which converged after approximately 96 kilometers.

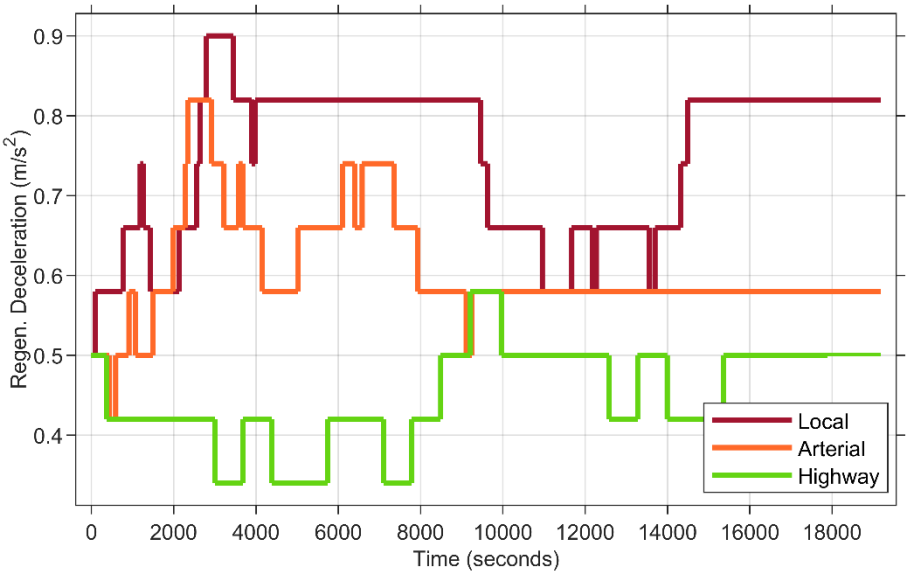

Figure 34. Online learning of optimal regenerative braking deceleration rates during repeated UDDS drive cycles.

Recall the driver intervention score objective functions associated with each driving condition of the UDDS drive cycle (Figure 21). We can assess the optimality of the Q-learning agent's converged deceleration values by comparing them with the known peaks of each objective function. Table 12 presents a comparison between the regenerative deceleration rates selected by the agents during online learning and the true optimum determined from the peaks of the objective functions. All three agents converged to within one 0.08 m/s^2 step of the optimal peaks, resulting in errors 0.0 %, 12.1 %, and 7.4 % for local, arterial, and highway driving conditions, respectively. This confirms that the ARB control scheme can effectively use online learning to locate the optimal deceleration rates within the search space with acceptable accuracy.

Table 12. Comparison of learned and true optimal regenerative braking decelerations identified in UDDS drive cycle.

Driving Condition	Regen. Deceleration (m/s^2)	
	Learned Optimum	**True Optimum**
Local	0.82	0.82
Arterial	0.58	0.66
Highway	0.50	0.54

To verify whether the ARB control scheme achieves a reduction in driver interventions throughout the simulated UDDS cycles, a moving average of the driver intervention score for each driving condition was logged. The same number of drive cycles was then repeated using two baseline regenerative braking control schemes; one using a conservative constant regenerative braking deceleration of 0.5 m/s^2 (CRB_0.5), and the other using an aggressive constant regenerative braking deceleration of 1.6 m/s^2 (CRB_1.6), commonly used by manufacturers.

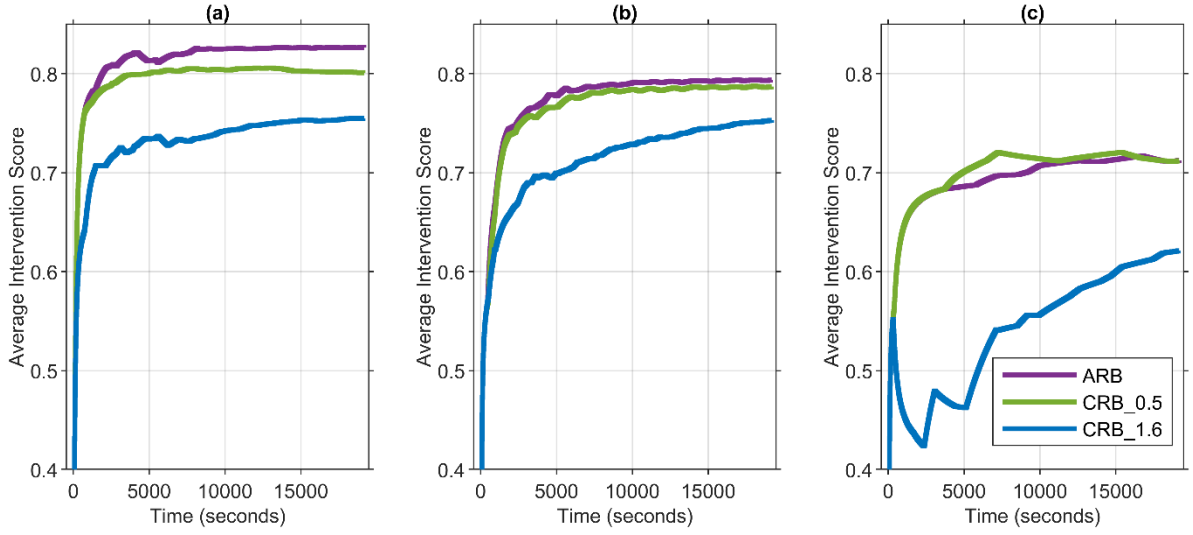

Figure 35. Plots of average driver intervention score across UDDS drive cycles for (a) local, (b) arterial, and (c) highway driving conditions.

Figure 35 illustrates the average driver intervention plots for each of the three regenerative braking control schemes across all driving conditions. The ARB control scheme displayed the highest driver intervention scores compared to the two baselines in local and arterial driving conditions. The most notable improvement in driver intervention score was observed in local driving conditions, likely explained by the Q-learning agent's convergence to the exact peak of the objective function. In highway driving, both the ARB and CRB_0.5 schemes eventually converged to a nearly identical driver intervention score since the ARB controller eventually settled on the same 0.5 m/s^2 deceleration rate as the CRB_0.5 scheme. The sharp variations in driver intervention scores for the CRB_1.6 controller in highway conditions were attributed to the driver model's constant micro-adjustments compensating for the aggressive lift-off deceleration. Although this behavior decreased over the drive cycle, it cannot be deemed representative of a human driver's pedal interactions.

Across all driving conditions, the more aggressive lift-off regenerative braking deceleration led to the highest level of driver intervention (i.e., the lowest driver intervention score). This is attributed to the need for the driver model to keep correcting the deceleration overshoot caused by lift-off regenerative braking. This finding is in line with the literature review, which indicated that some drivers view common implementations of lift-off regenerative braking to be too strong.

Table 13. Summary of results from ARB controller simulations.

Drive Cycle	**Driving Condition**	**Learned Optimum Decel. (m/s^2)**	**Decel. Error (%)**	**Final ARB Intervention Score**	**Final CRB_0.5 Intervention Score**	**Final CRB_1.6 Intervention Score**
UDDS	Local	0.82	0.0	0.827	0.801	0.755
	Arterial	0.58	12.1	0.793	0.787	0.753
	Highway	0.50	7.4	0.712	0.712	0.621
WLTC	Local	0.82	5.1	0.883	0.859	0.816
	Arterial	0.50	13.8	0.811	0.809	0.727
	Highway	0.50	13.8	0.715	0.708	0.630

This aforementioned simulation process was repeated for the WLTC drive cycle in order to corroborate the findings from the UDDS simulations. A summary of the results for both drive cycles simulations is included in Table 13. The Q-learning agents of the ARB controller converged to within one 0.08 m/s^2 step across all driving conditions in both drive cycles. The ARB control scheme outperformed the constant regenerative braking baseline schemes in all but one drive cycle – driving condition pairs, the exception being the nearly identical scores from the highway conditions in the UDDS drive cycles. The most significant improvement over the industry-standard CRB_1.6 variant occurred in the highway driving conditions of UDDS, showing a 14.7% improvement in the driver intervention score.

These results indicate that the ARB control scheme shows potential in achieving the goal of learning an optimal lift-off regenerative braking deceleration to minimize pedal usage, thereby improving the driving experience by reducing driver fatigue. The next phase of testing involves assessing the ARB controller's performance with a human driver performing a real-world drive cycle where no two deceleration events are identical.

4.2.2 Experimental Results

The complete ARB scheme integrated within the vehicle torque controller was flashed onto the supervisory controller of the UWAFT test vehicle. The same driver that was used to collect real-world data throughout this research performed a drive cycle of local driving conditions where laps of Route A were completed until the convergence of the ARB output. As with the simulation testing, the convergence criterion was two complete laps of Route A with no changes to the regenerative braking deceleration. The desired deceleration as well as the driver intervention score calculated by the ARB controller at every five deceleration events was logged throughout the drive cycle.

Table 14. Comparison of learned and true optimal regenerative braking decelerations identified in real-world local drive cycle.

Regen. Deceleration (m/s^2)	
Learned Optimum	**True Optimum (Estimated)**
0.74	0.73

The resulting performance of the ARB controller is illustrated in Figure 36. The desired regenerative braking deceleration converged to a value of 0.74 m/s^2 after 10 laps of Route A, equating to approximately 25 kilometers of driving. Recall that the objective functions of driver intervention score for the test driver used in this study were collected on two real-world local drive cycles. As outline in Table 14, these objective functions had a global peak at 0.76 m/s^2 and a local peak at 0.70 m/s^2, respectively. Taking the average of these two values yields an estimated global preference of lift-off regenerative braking deceleration of 0.73 m/s^2. This represents only a 1.4 % error between the learned optimum and the estimated true optimum for the test driver's preferred regenerative braking deceleration in local driving conditions. This suggests that despite driving on different routes across different individual drive cycles, the driver's global preference for that driving condition can be accurately identified by the ARB controller.

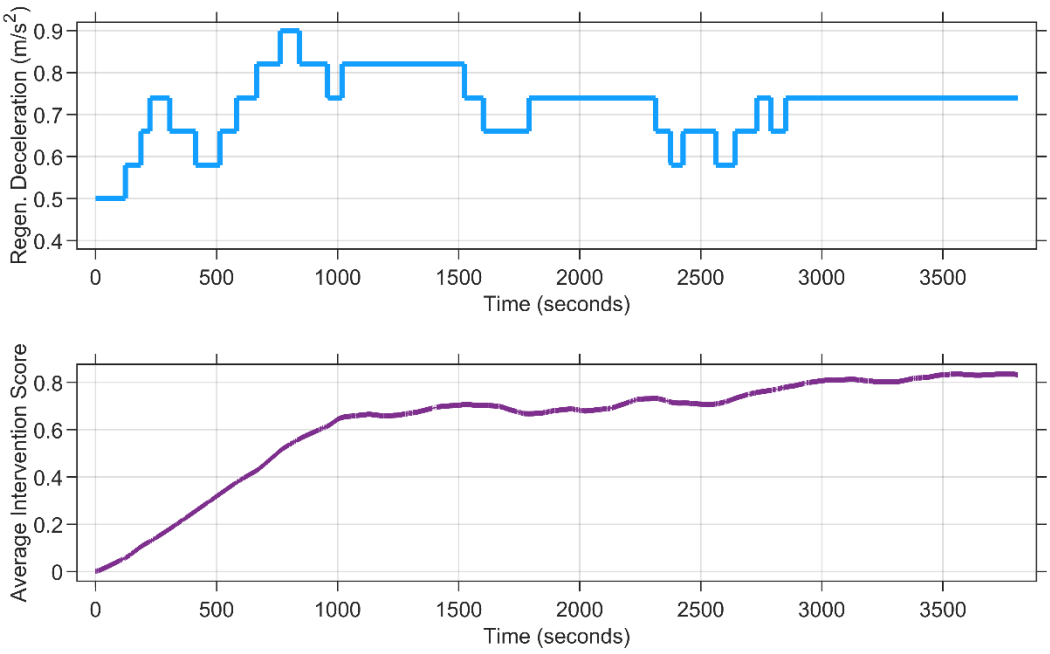

Figure 36. ARB performance throughout local real-world drive cycle.

The ARB controller calculates the driver intervention score in step-wise changes after every five deceleration events. This paired with the fact that the scores often fluctuate between sets of deceleration events means that the raw data is difficult to interpret visually. To address this, the logged scores are postprocessed to showcase the moving average of the driver intervention scores over the entire drive cycle. Figure 36 demonstrates this clearly, displaying how the average

intervention score rises over time. This upward trend suggests that the ARB controller effectively learned the driver's preferred deceleration rate, resulting in a reduced frequency of driver intervention during deceleration events.

To confirm the efficacy of the ARB controller in minimizing driver interventions as compared to baseline schemes employing constant deceleration rates, Route A was re-driven using the CRB_0.5 and CRB_1.6 variants, respectively. Since these drive cycles did not have a convergence criterion, Route A was only lapped three times. Subsequently, the driver interventions from these drive cycles were compared with the final three laps of the ARB drive cycle. The mean driver intervention scores across the last three laps of the ARB, CRB_0.5, and CRB_1.6 drive cycles are tabulated in Table 15. Notably, the ARB controller exhibited a significant improvement to driver intervention score compared to all other variants of the regenerative braking controller, outperforming the CRB_0.5 and CRB_1.6 variants by 8.5 % and 23.2 %, respectively. This finding validates that as the ARB controller approaches convergence, it effectively minimizes driver interventions, unlike baseline schemes that use constant decelerations not tailored to the driver's preferences.

Table 15. Mean driver intervention scores for final 3 laps of real-world local drive cycles using different regenerative braking control schemes.

Regenerative Braking Control Scheme	Mean Driver Intervention Score
ARB	0.829
CRB_0.5	0.764
CRB_1.6	0.673

The real-world experimentation with the proposed ARB controller indicates its successful adaptation to individual driver preferences, effectively reducing interventions with the accelerator and brake pedals during deceleration events. Compared to baseline schemes with constant regenerative braking rates, the ARB control shows potential for decreasing driver fatigue and enhancing the electrified vehicle driving experience. These findings affirm that the adaptive regenerative braking scheme fulfills the outlined research objectives. It's important to note that this experiment, involving a single test driver on a local route, isn't exhaustive. With that said, these promising results can be further reinforced through expanded studies with multiple subjects and diverse driving environments.

Chapter 5
Conclusion

The customization and adaptation of a vehicle's driving experience specific to each driver has become an increasing focus in modern vehicles. With the growing popularity of electrified vehicles, drivers are frequently interacting with various implementations of regenerative braking systems, such as lift-off regenerative braking. Since studies have shown that drivers are frequently uncomfortable or otherwise unsatisfied with the vehicle's predefined deceleration response during lift-off regenerative braking, this research sought to develop a regenerative braking control system that could learn and adapt to the driver's deceleration preferences. The primary objective was to enhance the driving experience and alleviate driver fatigue by minimizing pedal usage during braking.

To accomplish this objective, the research focused on three critical aspects: the accurate identification of current driving conditions for adaptive adjustments in regenerative braking strength, the acquisition of the driver's preferred lift-off regenerative braking deceleration to minimize pedal usage, and the compatibility of the proposed control scheme with real-time operations on standard automotive embedded hardware.

The first of these aspects was addressed by applying sophisticated techniques such as the HDBSCAN clustering algorithm and fuzzy logic inference to develop an online driving condition identifier. The identification system used data from an HDBSCAN cluster analysis to inform the construction of a fuzzy logic system to accurately identify driving conditions in 500-meter intervals as the vehicle is driven. The second aspect was addressed by developing an adaptive regenerative braking controller that used reinforcement learning to acquire an accurate estimate of the driver's preferred deceleration strength for a particular driving condition. This was done by applying the online Q-learning algorithm, whose learning was guided by a novel reward function based on the driver's interventions with the pedals during deceleration events. The third aspect was addressed by combining the online driving condition identifier with the adaptive regenerative braking controller and integrating the combined control system into the embedded hardware of an electrified test vehicle and testing its performance. The testing performed in this research was done in a MATLAB/Simulink simulation phase followed by a real-world experimentation phase using the electrified test vehicle on public roads.

The research outcomes demonstrate the efficacy of the HDBSCAN-informed fuzzy inference system (FIS) employed by the online driving condition identifier. When compared with a baseline identification scheme based solely on measurements of average velocity, the proposed online driving condition identifier exhibited enhanced stability, as evidenced by reduced sensitivity to velocity fluctuations and minimized driving condition label transitions. The application of the FIS-based online driving condition identifier also led to a high identification accuracy of 80.9 % in real-world experimentation, Notably, this represents a 6.8 % increase over the baseline. These findings highlight the significance of utilizing a broad range of vehicle data to identify driving conditions, reducing the system's sensitivity to individual measurements and ensuring a stable driving condition signal. This stability is crucial for improving the driving experience, as fluctuations could lead to unpredictable and uncomfortable driving behavior due to changes in the selected lift-off regenerative braking strength. The successful implementation of the online driving condition identifier on automotive-standard embedded hardware, coupled with its precise driving condition identification facilitated by the innovative application of the HDBSCAN clustering algorithm, has met the stipulated research objectives specific to the online driving condition identifier.

The testing of the adaptive regenerative braking (ARB) controller yielded promising results, demonstrating the controller’s ability to converge to a driver’s preference for deceleration. Simulation testing across UDDS and WLTC drive cycles showcased the ARB controller's ability to effectively converge to stable regenerative braking deceleration rates for each driving condition and reduce the average driver intervention score, thereby suggesting an enhancement of driving comfort. Real-world experimentation on a local road segment further confirmed the controller's capability to adapt to individual driver preferences, with the ARB controller converging to within 1.4 % of an individual driver’s estimated deceleration preference for local driving conditions. In doing so, the ARB controller significantly outperformed baseline schemes using constant deceleration rates in the reduction of indicators of driver fatigue. Notably, the ARB controller demonstrates a substantial 23.2 % reduction in driver interventions over a baseline scheme employing a constant deceleration rate which is representative of typical implementations used by manufacturers. This underscores the ARB controller’s potential to mitigate driver fatigue and improve the overall driving experience for electrified vehicles. These findings affirm the ARB control scheme's success in meeting the outlined research objectives. It highlights the scheme's ability to adapt to individual driver preferences, reduce

the frequency of driver interventions during deceleration events, and enhance overall driving comfort in a real-time automotive application on a vehicle's embedded controller.

By effectively achieving the outlined research objectives, this study has significantly propelled the advancement of electrified vehicle powertrain control. This research places a specific emphasis on increasing the acceptance and driver satisfaction of regenerative braking systems, an aspect often overshadowed in research in favor of efficiency optimization. The application of advanced methodologies such as the HDBSCAN clustering algorithm, fuzzy logic inference, and the online Q-learning algorithm represents a significant contribution to the progress and refinement of contemporary electrified vehicle powertrain control technologies.

5.1 Limitations

While the research presents a promising proof of concept, it is not without its limitations. Given that the primary objective of this study was centered on the design of an advanced controller to enhance the driving experience in electrified vehicles, an apparent limitation pertains to a lack of test subjects and environments in order to investigate human interactions with the proposed ARB controller. While the study successfully demonstrates the technical feasibility and effectiveness of the ARB controller in simulation as well as in experiments with an individual test driver, the absence of a comprehensive human-centered study limits the extent to which the study's findings can be generalized to real-world practical driving. The author of this thesis thus acknowledges the need for further comprehensive studies involving multiple test subjects and diverse driving environments to solidify the effectiveness and applicability of the proposed ARB control scheme in practical scenarios.

5.2 Future Work

The successful development and validation of the ARB control system has laid a solid foundation for future research endeavors aimed at further enhancing the driving experience in electrified vehicles. Building upon the insights gained from this study, several areas for future research into driver-focused regenerative braking optimization emerge, such as comprehensive human-centered studies and integration with advanced driver-assistance systems (ADAS).

As highlighted in the limitations, conducting human-centered studies involving a larger sample of test drivers and varied driving conditions would further evaluate the ARB controller's ability to

reduce driver fatigue and improve the acceptance of lift-off regenerative braking systems. Further research should prioritize comprehensive investigations to assess driver interaction, satisfaction, and overall user experience with the ARB control scheme. This can include longitudinal studies whereby driver behaviour and user satisfaction are monitored over an extended period.

Given the increasing prevalence of ADAS in modern vehicles, future research should explore how an adaptive regenerative braking control system might integrate with existing ADAS technologies. Exploring the interplay between these control systems would contribute to a holistic approach to vehicle control, aiming to enhance the overall driving experience through seamless coordination among various adaptive control systems. Such exploration can lead to valuable insights on how the collaboration between these systems can be leveraged to improve driving safety and comfort, ultimately contributing to the advancement of vehicle control technology

In conclusion, by addressing these critical research areas in the future, the proposed ARB control system can be further refined and optimized to improve the driving experience. This effort will not only contribute to the maturation of regenerative braking control systems, but also to the advancement and widespread adoption of electrified vehicle technologies as a whole.

References

[1] Bartlett, J., and Preston, B. “Automakers Are Adding Electric Vehicles to Lineups.” Consumer Reports. Accessed November 8, 2023. https://www.consumerreports.org/cars/hybrids-evs/why-electric-cars-may-soon-flood-the-us-market-a9006292675/.

[2] “Electrified Vehicles.” Carnegie Mellon University Vehicle Electrification Group. Accessed November 8, 2023. https://www.cmu.edu/cit/veg/electrified%20vehicles/index.html.

[3] “Types of Electric Vehicles.” J.D. Power. Accessed November 8, 2023. https://www.jdpower.com/cars/shopping-guides/types-of-electric-vehicles-mild-hybrid-hybrid-plug-in-hybrid-and-electric.

[4] “Factors Contributing to a Growing Electric Vehicle Market.” U.S. Bureau of Labor Statistics. Accessed November 8, 2023. https://www.bls.gov/opub/btn/volume-12/charging-into-the-future-the-transition-to-electric-vehicles.htm.

[5] Kampker, A., Offermanns, C., Heimes, H., and Bi, P. “Meta-Analysis on the Market Development of Electrified Vehicles.” *ATZ Worldwide* 123, no. 7–8 (2021): 58–63. https://doi.org/10.1007/s38311-021-0685-7.

[6] Haghani, M., Sprei, F., Kazemzadeh, K., Shahhoseini, Z., and Aghaei, J. “Trends in Electric Vehicles Research.” *Transportation Research Part D: Transport and Environment* (2023): 103881. https://doi.org/10.1016/j.trd.2023.103881.

[7] Chuanwei, Z., Zhifeng, B., Binggang, C., Jingcheng, L., "Study on regenerative braking of electric vehicle," The 4th International Power Electronics and Motion Control Conference, 2004. IPEMC 2004., Xi'an, China, 2004, pp. 836- 839 Vol.2.

[8] Sangtarash, F., Esfahanian, V., Nehzati, H., Haddadi, S., Bavanpour, M., and Haghpanah, B. “Effect of Different Regenerative Braking Strategies on Braking Performance and Fuel Economy in a Hybrid Electric Bus Employing Cruise Vehicle Simulation.” *SAE International Journal of Fuels and Lubricants* 1, no. 1 (2008): 828–37. https://doi.org/10.4271/2008-01-1561.

[9] Xu, G., Xu, K., Zheng, C., Zhang, X., and Zahid, T. “Fully Electrified Regenerative Braking Control for Deep Energy Recovery and Maintaining Safety of Electric Vehicles.” *IEEE Transactions on Vehicular Technology* 65, no. 3 (2016): 1186–98. https://doi.org/10.1109/tvt.2015.2410694.

[10] Rahul, G., Yadav, R., Yadav, R., and Chawla, D. “The Advancement of United Acceleration–Brake Pedal: A Review.” *Advances in Engineering Design*, 2019, 311–20. https://doi.org/10.1007/978-981-13-6469-3_28.

[11] Liu, W., Qi, H., Liu, X., and Wang, Y. “Evaluation of Regenerative Braking Based on Single-Pedal Control for Electric Vehicles.” *Frontiers of Mechanical Engineering* 15, no. 1 (2019): 166–79. https://doi.org/10.1007/s11465-019-0546-x.

[12] “Model 3 Owner’s Manual.” Tesla. Accessed November 8, 2023. https://www.tesla.com/ownersmanual/model3/en_us/.

[13] “EV6 Manual: Adjusting regenerative braking with paddle shifter.” Kia. Accessed November 8, 2023. https://www.kia.com/content/dam/kia2/in/en/content/ev6-manual/topics/chapter6_4_1.html.

[14] “EQS Operator’s Manual.” Mercedes-Benz. Accessed November 8, 2023. mbusa.com/content/dam/mb-nafta/us/owners/manuals/2022/OperatorManuals/EQS Owners Manual.pdf

[15] “2023 LEAF Owner’s Manual.” Nissan. Accessed November 8, 2023. https://www.nissan.ca/content/dam/Nissan/Canada/manuals-and-guides/leaf/2023/2023-nissan-Leaf-en.pdf

[16] Oleksowicz, S., Burnham, K., Southgate, A., McCoy, C., Waite, G., Hardwick, G., Harrington, C., and McMurran, R. “Regenerative Braking Strategies, Vehicle Safety and Stability Control Systems: Critical Use-Case Proposals.” *Vehicle System Dynamics* 51, no. 5 (2013): 684–99. https://doi.org/10.1080/00423114.2013.767462.

[17] Borgia, F. and Samuel, S., "Design of Drive Cycle for Electric Powertrain Testing," SAE Technical Paper 2023-01-0482, 2023. https://doi.org/10.4271/2023-01-0482.

[18] RT, S., Bose, A., and Ibrahim, M., "Condensation of Real-World Drive Cycle into Synthetic Drive Cycle - An Innovative Method to Predict Real Driving Emissions," SAE Technical Paper 2021-01-0602, 2021. https://doi.org/10.4271/2021-01-0602.

[19] Gebisa, A., Girma G., Rajendiran G., and Ramesh B. N., "Driving Cycles for Estimating Vehicle Emission Levels and Energy Consumption" *Future Transportation* 1, no. 3: 615-638, 2021. https://doi.org/10.3390/futuretransp1030033.

[20] "Urban Dynamometer Driving Schedule (UDDS)", U.S. Environmental Protection Agency. Accessed November 8, 2023. https://www.epa.gov/emission-standards-reference-guide/epa-urban-dynamometer-driving-schedule-udds

[21] Davari, M., Jerrelind, J., and Stensson-Trigell, A. "Energy Efficiency Analyses of a Vehicle in Modal and Transient Driving Cycles Including Longitudinal and Vertical Dynamics." *Transportation Research Part D: Transport and Environment* 53 (2017): 263–75. https://doi.org/10.1016/j.trd.2017.04.019.

[22] Yang, J., Millichamp, J., Suter, T., Shearing, P., Brett, D., and Robinson, J. "A Review of Drive Cycles for Electrochemical Propulsion." *Energies* 16, no. 18 (2023): 6552. https://doi.org/10.3390/en16186552.

[23] Yusof, N., Abas, M., Rohana, N., and Perang, M. "Route Selection for Road Vehicle Real-Driving Emissions Test Using GIS." *IOP Conference Series: Earth and Environmental Science* 1143, no. 1 (2023): 012027. https://doi.org/10.1088/1755-1315/1143/1/012027.

[24] Wang, R., and Lukic, S. "Review of Driving Conditions Prediction and Driving Style Recognition Based Control Algorithms for Hybrid Electric Vehicles." *IEEE Vehicle Power and Propulsion Conference*, 2011. https://doi.org/10.1109/vppc.2011.6043061.

[25] Ravi, S., and Marco, J. "Method for Estimating the Energy Consumption of Electric Vehicles and Plug-in Hybrid Electric Vehicles under Real-world Driving Conditions." *IET Intelligent Transport Systems* 7, no. 1 (2013): 138–50. https://doi.org/10.1049/iet-its.2012.0114.

[26] Hou, Z., Guo, J., Xing, J., Guo, C., and Zhang, Y. "Machine Learning and Whale Optimization Algorithm Based Design of Energy Management Strategy for Plug-in Hybrid Electric Vehicle." *IET Intelligent Transport Systems* 15, no. 8 (2021): 1076–91. https://doi.org/10.1049/itr2.12084.

[27] Song, J., and Cha, J. “Analysis of Driving Dynamics Considering Driving Resistances in On-Road Driving.” *Energies* 14, no. 12 (2021): 3408. https://doi.org/10.3390/en14123408.

[28] Popiv, D., Rommerskirchen, C., Rakic, M., Duschl, M., Bengler, K.,“Effects of assistance of anticipatory driving on drivers behaviour during deceleration phases,” in *European conference on human centered designfor intelligent transport systems*, (2010): 29–30.

[29] Szumska, E., and Jurecki, R. “The Analysis of Energy Recovered during the Braking of an Electric Vehicle in Different Driving Conditions.” *Energies* 15, no. 24 (2022): 9369. https://doi.org/10.3390/en15249369.

[30] “Kia Niro Owner’s Manual.” Kia. Accessed November 8, 2023. https://www.kia.com/content/dam/kwcms/au/en/files/owners-manual/niro/kia-niro-pbv-owners-manual-my23.pdf

[31] Berjoza, D., Pirs, V., and Jurgena, I. “Research into the Regenerative Braking of an Electric Car in Urban Driving.” *World Electric Vehicle Journal* 13, no. 11 (2022): 202. https://doi.org/10.3390/wevj13110202.

[32] Van Boekel, J.J.P., Besselink, I.J.M, and Nijmeijer H., “Design and Realization of a One-Pedal-Driving Algorithm for the TU/e Lupo El.” *World Electric Vehicle Journal* 7, no. 2: 226–37, 2015. https://doi.org/10.3390/wevj7020226.

[33] Cocron, P., Bühler, F., Franke, T., Neumann, I., Dielmann, D., and Krems, J. “Energy Recapture through Deceleration – Regenerative Braking in Electric Vehicles from a User Perspective.” *Ergonomics* 56, no. 8 (2013): 1203–15. https://doi.org/10.1080/00140139.2013.803160.

[34] Tong, H.Y., and Hung, W.T. “A Framework for Developing Driving Cycles with On-road Driving Data.” *Transport Reviews* 30, no. 5 (2010): 589–615. https://doi.org/10.1080/01441640903286134.

[35] Huzayyin, O., Salem, H., and Hassan, M. “A Representative Urban Driving Cycle for Passenger Vehicles to Estimate Fuel Consumption and Emission Rates under Real-World Driving Conditions.” *Urban Climate* 36 (2021): 100810. https://doi.org/10.1016/j.uclim.2021.100810.

[36] Liessner, R. Dietermann, A., Bäker, B., and Lüpkes, K. "Generation of replacement vehicle speed cycles based on extensive customer data by means of Markov models and threshold accepting", *SAE Int. J. Alternative Powertrains*, vol. 6, no. 1, pp. 165-173, 2017.

[37] Pfriem, M., and Gauterin, F. "Development of real-world driving cycles for battery electric vehicles", *World Electric Vehicle J.*, vol. 8, pp. 14-24, 2016.

[38] Förster, D., Inderka, R.B., and Gauterin, F., "Data-Driven Identification of Characteristic Real-Driving Cycles Based on k-Means Clustering and Mixed-Integer Optimization," in *IEEE Transactions on Vehicular Technology*, vol. 69, no. 3, pp. 2398-2410, 2020. https://doi.org/10.1109/TVT.2019.2963272.

[39] Hu, J., Liu, D., Du, C., Yan, F., and Lv, C., "Intelligent Energy Management Strategy of Hybrid Energy Storage System for electric vehicle based on driving pattern recognition," *Energy*, vol. 198, p. 117298, 2020.

[40] Lee, T. -K., Adornato, B., and Filipi, Z. S., "Synthesis of Real-World Driving Cycles and Their Use for Estimating PHEV Energy Consumption and Charging Opportunities: Case Study for Midwest/U.S.," in *IEEE Transactions on Vehicular Technology*, vol. 60, no. 9, pp. 4153-4163, 2011. https://doi.org/10.1109/TVT.2011.2168251.

[41] Shahidinejad, S., Bibeau, E., and Filizadeh, S., "Statistical Development of a Duty Cycle for Plug-in Vehicles in a North American Urban Setting Using Fleet Information," in *IEEE Transactions on Vehicular Technology*, vol. 59, no. 8, pp. 3710-3719, 2010. https://doi.org/10.1109/TVT.2010.2061243.

[42] Xu, D. and Tian, Y., "A comprehensive survey of clustering algorithms", *Ann. Data Sci.*, vol. 2, no. 2, pp. 165-193, 2015.

[43] Hou, Z., Guo, J., Xing, J., Guo, C., and Zhang, Y., "Machine Learning and Whale Optimization Algorithm Based Design of Energy Management Strategy for Plug-in Hybrid Electric Vehicle." *IET Intelligent Transport Systems* 15, no. 8: 1076–91, 2021. https://doi.org/10.1049/itr2.12084.

[44] Jain, A., Hautier, G., Ong, S. P., and Persson, K., "New opportunities for materials informatics: Resources and data mining techniques for uncovering hidden relationships," *Journal of Materials Research*, vol. 31, no. 8, pp. 977–994, 2016.

[45] Humaira, H. and Rasyidah, R., “Determining the Appropriate Cluster Number Using Elbow Method for K-Means Algorithm”, *Proceedings of the 2nd Workshop on Multidisciplinary and Applications,* 2018. https://doi.org/10.4108/eai.24-1-2018.2292388.

[46] Nelles, O., “Nonlinear System Identification: From Classical Approaches to Neural Networks and Fuzzy Models”, Berlin: Springer, 2001. ISBN 978-3-020-47438-6.

[47] Mohiuddin, A., Seraj, R., and Mohammed, S., "The *k-means* Algorithm: A Comprehensive Survey and Performance Evaluation" *Electronics* 9, no. 8: 1295, 2020. https://doi.org/10.3390/electronics9081295.

[48] Ertöz, L., Steinbach, M., and Kumar, V., “Finding clusters of different sizes, shapes, and densities in noisy, high dimensional data,” *Proceedings of the 2003 SIAM International Conference on Data Mining*, 2003. https://doi.org/10.1137/1.9781611972733.5.

[49] McInnes, L., Healy, J., and Astels, S., “HDBSCAN Documentation”. Accessed November 8, 2023. https://hdbscan.readthedocs.io/_/downloads/ en/0.8.18/pdf/.

[50] Campello, R., Moulavi, D., and Sander, J., “Density-based clustering based on hierarchical density estimates.” *Pacific-Asia conference on knowledge discovery and data mining*. Springer, Berlin, Heidelberg, 2013. https://doi.org/10.1007/978-3-642-37456-2_14.

[51] Zhang, X., Huang , Y., Guo, K., and Li, W., "Driving Style Classification for Vehicle-Following with Unlabeled Naturalistic Driving Data," 2019 IEEE Vehicle Power and Propulsion Conference (VPPC), Hanoi, Vietnam, pp. 1-5, 2019. https://doi.org/10.1109/VPPC46532.2019.8952462.

[52] Wang, R., Zheng, W., Huang, M., and Li, G., "Driving Behavior Evaluation Based on DBSCAN and Kmeans++ Clustering," 2022 5th International Conference on Advanced Electronic Materials, Computers and Software Engineering (AEMCSE), Wuhan, China, pp. 188-193, 2022. https://doi.org/10.1109/AEMCSE55572.2022.00046.

[53] Yang, D.P., Liu, T., Zhang, X.M., Zeng, X.H., and Song, D.F., “Construction of High-Precision Driving Cycle Based on Metropolis-Hastings Sampling and Genetic Algorithm.” *Transportation Research Part D: Transport and Environment* 118: 103715, 2023. https://doi.org/10.1016/j.trd.2023.103715.

[54] Faraji-Niri, M., Dinh, T. Q., and Marco, J., "Riding Pattern Identification by Machine Learning for Electric Motorcycles," 24th International Conference on Mechatronics Technology (ICMT), Singapore, pp. 1-6, 2021. https://doi.org/10.1109/ICMT53429.2021.9687179.

[55] Afifi, S., Gholam-Hosseini, H., and Sinha, R., "FPGA Implementations of SVM Classifiers: A Review." *SN Computer Science* 1, no. 3, 2020. https://doi.org/10.1007/s42979-020-00128-9.

[56] Pires, P.B., and Santos, J.D. "Artificial Intelligence and Marketing: Progressive or Disruptive Transformation? Review of the Literature." *Confronting Security and Privacy Challenges in Digital Marketing,* edited by Paulo Botelho Pires, et al., IGI Global, 2023, pp. 95-118. https://doi.org/10.4018/978-1-6684-8958-1.ch005

[57] Von Altrock, C. "Fuzzy Logic Technologies in Automotive Engineering." *IEEE Proceedings of WESCON*, 1994. https://doi.org/10.1109/wescon.1994.403618.

[58] Schüler, M., Onnen, C., and Bielaczek, C. "A Fuzzy-System for a Classification of the Driver Behavior and the Driving Situation." *IFAC Proceedings Volumes* 30, no. 8 (1997): 693–98. https://doi.org/10.1016/s1474-6670(17)43901-2.

[59] Zhang, S., and Xiong, R. "Adaptive Energy Management of a Plug-in Hybrid Electric Vehicle Based on Driving Pattern Recognition and Dynamic Programming." *Applied Energy* 155 (2015): 68–78. https://doi.org/10.1016/j.apenergy.2015.06.003.

[60] Bellem, H., Thiel, B., Schrauf, M., and Krems, J. "Comfort in Automated Driving: An Analysis of Preferences for Different Automated Driving Styles and Their Dependence on Personality Traits." *Transportation Research Part F: Traffic Psychology and Behaviour* 55 (2018): 90–100. https://doi.org/10.1016/j.trf.2018.02.036.

[61] Butakov, V., and Ioannou, P. "Personalized Driver Assistance for Signalized Intersections Using V2i Communication." *IEEE Transactions on Intelligent Transportation Systems* 17, no. 7 (2016): 1910–19. https://doi.org/10.1109/tits.2016.2515023.

[62] Bosetti, P., Da Lio, M., and Saroldi, A. "On the Human Control of Vehicles: An Experimental Study of Acceleration." *European Transport Research Review* 6, no. 2 (2013): 157–70. https://doi.org/10.1007/s12544-013-0120-2.

[63] Yavas, M., Kumbasar, U., and Ure, N.K. “Toward Learning Human-like, Safe and Comfortable Car-Following Policies with a Novel Deep Reinforcement Learning Approach.” *IEEE Access* 11 (2023): 16843–54. https://doi.org/10.1109/access.2023.3245831.

[64] Wortman, R.H., and Fox, T. “An Evaluation of Vehicle Deceleration Profiles.” *Journal of Advanced Transportation* 28, no. 3 (1994): 203–15. https://doi.org/10.1002/atr.5670280303.

[65] Wallace, B., Puli, A., Goubran, R., Knoefel, F., Marshall, S., Porter, M., and Smith, A. “Big Data Analytics to Identify Deceleration Characteristics of an Older Driver.” *2015 IEEE International Symposium on Medical Measurements and Applications (MeMeA) Proceedings*, 2015. https://doi.org/10.1109/memea.2015.7145178.

[66] Yang, L. “Driver Speed and Acceleration Behaviour on Canadian Roads.” *Carleton University*, 2007.

[67] Deligianni, S.P., “Modelling Drivers’ Braking Behaviour and Comfort Under Normal Driving.” *Loughborough University*, 2019.

[68] Reinolsmann, N., Alhajyaseen, W., Brijs, T., Pirdavani, A., Hussain, Q., and Brijs, K. “Investigating the Impact of a Novel Active Gap Metering Signalization Strategy on Driver Behavior at Highway Merging Sections.” *Transportation Research Part F: Traffic Psychology and Behaviour* 78 (2021): 42–57. https://doi.org/10.1016/j.trf.2021.01.017.

[69] Schmitz, M. , Jagiellowicz, M., Maag, C., and Hanig, M. “The Impact of Different Pedal Solutions for Supporting Efficient Driving with Electric Vehicles.” in *Proceedings of European Conference on Human Centered Design for Intelligent Transport Systems (HUMANIST)*. Lyon: Humanist Publications, 2012.

[70] Eberl, T., Sharma, R., Stroph, R., Schumann, J., and Pruckner, A. “Evaluation of Interaction Concepts for the Longitudinal Dynamics of Electric Vehicles.” In *Advances in Human Factors and Ergonomics 2012–2014 Volume Set: Proceedings of the 4th AHFE Conference July 21–25, 2012*. San Francisco: CRC Press, 2012.

[71] Kim, D., Soo Eo, J., and Kim, K. “Parameterized Energy-Optimal Regenerative Braking Strategy for Connected and Autonomous Electrified Vehicles: A Real-Time Dynamic Programming Approach.” *IEEE Access* 9 (2021): 103167–83. https://doi.org/10.1109/access.2021.3098807.

[72] Moon, S., and Yi, K. “Human Driving Data-Based Design of a Vehicle Adaptive Cruise Control Algorithm.” *Vehicle System Dynamics* 46, no. 8 (2008): 661–90. https://doi.org/10.1080/00423110701576130.

[73] Lian, Y., Zhao, Y., Hu, L., and Tian, Y. “Longitudinal Collision Avoidance Control of Electric Vehicles Based on a New Safety Distance Model and Constrained-Regenerative-Braking-Strength-Continuity Braking Force Distribution Strategy.” *IEEE Transactions on Vehicular Technology* 65, no. 6 (2016): 4079–94. https://doi.org/10.1109/tvt.2015.2498949.

[74] Chakraborty, D., and Nandi, A.K. “Finding Optimal Deceleration with Serial Regenerative Braking of Electric Vehicle Using a Multi-Objective Genetic Algorithm.” *2016 IEEE 1st International Conference on Power Electronics, Intelligent Control and Energy Systems (ICPEICES)*, 2016. https://doi.org/10.1109/icpeices.2016.7853333.

[75] Dehkordi, S.G., Cholette, M., Larue, G., Rakotonirainy, A., and Glaser, S. “Energy Efficient and Safe Control Strategy for Electric Vehicles Including Driver Preference.” *IEEE Access* 9 (2021): 11109–22. https://doi.org/10.1109/access.2021.3050780.

[76] Lin, X., and Li, H. “Adaptive Control Strategy Extracted from Dynamic Programming and Combined with Driving Pattern Recognition for Spheb.” *International Journal of Automotive Technology* 20, no. 5 (2019): 1009–22. https://doi.org/10.1007/s12239-019-0095-7.

[77] Huang, J., Chen, Y., Peng, X., Hu, L., and Cao, D. “Study on the Driving Style Adaptive Vehicle Longitudinal Control Strategy.” *IEEE/CAA Journal of Automatica Sinica* 7, no. 4 (2020): 1107–15. https://doi.org/10.1109/jas.2020.1003261.

[78] Kubaisi, R. “Adaptive Regenerative Braking in Electric Vehicles.” *Karlsruhe Institute of Technology*, 2018.

[79] Nelles, O. “IntelligenTip®: A Learning Driving Strategy for Automated Transmissions.” *SAE Technical Paper Series*, 2003. https://doi.org/10.4271/2003-01-0534.

[80] He, Y., Liu, Y., Yang, L., and Qu, X. “Deep Adaptive Control: Deep Reinforcement Learning-Based Adaptive Vehicle Trajectory Control Algorithms for Different Risk Levels.” *IEEE Transactions on Intelligent Vehicles*, 2023, 1–12. https://doi.org/10.1109/tiv.2023.3303408.

[81] Mnih, V., Kavukcuoglu, K., Graves, A., Antonoglou, I., Wierstra, D., and Riedmiller, M. "Playing Atari with Deep Reinforcement Learning." DeepMind Technologies, December 2013. https://doi.org/https://doi.org/10.48550/arXiv.1312.5602.

[82] "Vehicle Body 3DOF Longitudinal." MathWorks. Accessed November 8, 2023. https://www.mathworks.com/help/autoblks/ref/vehiclebody1doflongitudinal.html.

[83] "Mapped Motor." MathWorks. Accessed November 8, 2023. https://www.mathworks.com/help/autoblks/ref/mappedmotor.html

[84] MacAdam, Charles C. "Application of an Optimal Preview Control for Simulation of Closed-Loop Automobile Driving." *IEEE Transactions on Systems, Man, and Cybernetics* 11, no. 6 (1981): 393–99. https://doi.org/10.1109/tsmc.1981.4308705.

[85] Yang, D.P., Liu, T., Zhang, X.M., Zeng, X.H., and Song, D.F., "Construction of High-Precision Driving Cycle Based on Metropolis-Hastings Sampling and Genetic Algorithm." *Transportation Research Part D: Transport and Environment* 118: 103715, 2023. https://doi.org/10.1016/j.trd.2023.103715.

[86] Shahapure, K. R. and Nicholas C., "Cluster Quality Analysis Using Silhouette Score," *2020 IEEE 7th International Conference on Data Science and Advanced Analytics (DSAA)*, pp. 747-748, 2020. https://doi.org/10.1109/DSAA49011.2020.00096.

[87] "Ontario Road Network (ORN) Road Net Element." Ontario Ministry of Natural Resources and Forestry. Accessed November 8, 2023. https://geohub.lio.gov.on.ca/datasets/mnrf::ontario-road-network-orn-road-net-element/about.

[88] Lee, J.D., Liu, S.Y., Domeyer, J., and Dinparast-Djadid, A. "Assessing Drivers' Trust of Automated Vehicle Driving Styles with a Two-Part Mixed Model of Intervention Tendency and Magnitude." *Human Factors: The Journal of the Human Factors and Ergonomics Society* 63, no. 2 (2019): 197–209. https://doi.org/10.1177/0018720819880363.

[89] McLaughlin, S. "Measurement of Driver Preferences and Intervention Responses as Influenced by Adaptive Cruise Control Deceleration Characteristics." *Virginia Polytechnic Institute and State University,* 1998.

[90] Watkins, C. "Learning from Delayed Rewards." *King's College*, 1989.

[91] André, M., “The Artemis European Driving Cycles for Measuring Car Pollutant Emissions.” *Science of The Total Environment* 334–335: 73–84, 2004. https://doi.org/10.1016/j.scitotenv.2004.04.070.

[92] “Ontario Road Network (ORN) Road Net Element.” Ontario Ministry of Natural Resources and Forestry. Accessed November 8, 2023. https://geohub.lio.gov.on.ca/datasets/mnrf::ontario-road-network-orn-road-net-element/about

[93] Ponticel, P. “Heavy Brake Re-Gen Feel Dominates I3 Driving Experience.” Mobility Engineering Technology, June 12, 2023. https://www.mobilityengineeringtech.com/component/content/article/ae/stories/news/41263.

[94] “Worldwide Harmonised Light Vehicle Test Procedure.” United Nations Economic Commission for Europe. Accessed November 8, 2023. https://unece.org/DAM/trans/doc/2012/wp29grpe/WLTP-DHC-12-07e.xls

Appendix A:

Feature Values of HDBSCAN Clusters

Inferred Driving Condition	**Avg. Velocity (km/h)**	**Avg. Pos. Accel. (m/s^2)**	**Avg. Neg. Accel. (m/s^2)**	**Std. Velocity (km/h)**	**Std. Pos. Accel. (m/s^2)**	**Std. Neg. Accel. (m/s^2)**	**Max. Velocity (km/h)**	**Max. Pos. Accel. (m/s^2)**	**Max. Neg. Accel. (m/s^2)**	**Num. Stops**
Local	23.797	0.031	0.029	13.401	0.041	0.044	43.998	0.142	0.165	2
Arterial	31.406	0.026	0.026	14.218	0.037	0.040	48.135	0.135	0.148	1
Highway	93.932	0.007	0.006	1.655	0.009	0.009	96.398	0.030	0.031	0

Appendix B:

Q-Learning Algorithm Implementation

```
def qlearning(objective, iterations, n_episodes, step_size, label):
    epsilon = 1
    epsilon_decay = 0.3
    min_epsilon = 0.1
    gamma = 0.1
    lr = 0.1
    n_states = int((2-0.2)/min_step_size)
    n_actions = 3
    #Initialize Q-table
    Q_table = np.zeros((n_states,n_actions))
    #Starting point
    current_state = 0
    current_regen = 0.2
    next_state = 0
    prev_state = 0
    prev_score = 0
    prev_action = 1
    next_regen = 0.3
    best_score = 0
    best_state = 1
    best_regen = 0.3
    actions = ['NegStep', 'NoChange', 'PosStep']
    rewards_per_episode = list()

    for e in range (n_episodes):
        epsilon = round(max(min_epsilon, np.exp(-epsilon_decay*e)),2)
        lr = 0.1*np.exp(-0.1*e)
        total_episode_reward = 0

        for i in range(iterations):
            reward = 0
            score = objective(current_regen,label)[0]
            reward = (1-best_score/score)
            if score > best_score:
                best_score = score
                best_state = current_state
                best_regen = current_regen
            if score >= prev_score:
                reward = reward + 0.1
            else:
                reward = reward - 0.1
            if current_state == best_state:
                reward = reward + 0.1
            elif abs(best_state - current_state) < abs(best_state - prev_state):
                reward = reward + 0.1
```

```
            else:
                reward = reward - 0.1

            Q_table[prev_state, prev_action] = (1-lr) * Q_table[prev_state,
prev_action] + lr*(reward + gamma*np.max(Q_table[current_state,:]))

            if np.random.uniform(0,1) < epsilon:
                #Select random action
                action = actions.index(random.choice(actions))
            else:
                action = np.argmax(Q_table[current_state,:])

            if action == 0:
                next_state = current_state - 1
                next_regen = round(current_regen - step_size,2)
                if next_state < 0:
                    action = 2
            if action == 1:
                next_state = current_state
                next_regen = current_regen
            if action == 2:
                next_state = current_state + 1
                next_regen = round(current_regen + step_size,2)

            total_episode_reward = total_episode_reward + reward

            prev_state = current_state
            prev_regen = current_regen
            prev_action = action
            prev_score = score
            current_state = next_state
            current_regen = next_regen

        rewards_per_episode.append(total_episode_reward)

    return Q_table
```